Search for resonances decaying to a pair of Higgs bosons in the $\mathrm{b\bar{b}q\bar{q}'\ell\nu}$ final state in proton-proton collisions at $\sqrt{\mathrm{s}} = 13\,\mathrm{TeV}$

The CMS collaboration

E-mail: cms-publication-committee-chair@cern.ch

ABSTRACT: A search for new massive particles decaying into a pair of Higgs bosons in proton-proton collisions at a center-of-mass energy of 13 TeV is presented. Data were collected with the CMS detector at the LHC, corresponding to an integrated luminosity of $35.9\,\mathrm{fb}^{-1}$. The search is performed for resonances with a mass between 0.8 and 3.5 TeV using events in which one Higgs boson decays into a bottom quark pair and the other decays into two W bosons that subsequently decay into a lepton, a neutrino, and a quark pair. The Higgs boson decays are reconstructed with techniques that identify final state quarks as substructure within boosted jets. The data are consistent with standard model expectations. Exclusion limits are placed on the product of the cross section and branching fraction for generic spin-0 and spin-2 massive resonances. The results are interpreted in the context of radion and bulk graviton production in models with a warped extra spatial dimension. These are the best results to date from searches for an HH resonance decaying to this final state, and they are comparable to the results from searches in other channels for resonances with masses below 1.5 TeV.

Contents

1 Introduction

The discovery of a Higgs boson (H) [1–3] established the existence of at least a simple mass generation mechanism for the standard model (SM) [4, 5], the so-called "Higgs Mechanism". The simple model, however, has a number of limitations that are ameliorated [6] by a so-called "extended Higgs sector". Supersymmetry [7–14] requires such an extended Higgs sector, with new spin-0 particles. Another class of models with warped extra dimensions, proposed by Randall and Sundrum [15], postulates the existence of a compact fourth spatial dimension with a warped metric. Such compactification creates heavy resonances arising as

a tower of Kaluza-Klein excitations, leading to possible spin-0 radions [16–19] or spin-2 bulk gravitons [20–22]. The ATLAS [23–38] and CMS [39–57] collaborations have conducted a number of searches for these particles, where the new bosons decay into vector bosons and/or Higgs bosons (WW, ZZ, WZ, HH, ZH, or WH).

In this paper, we describe a search for narrow resonances (X) decaying to HH, where one H decays to a bottom quark pair ($b\overline{b}$) and the other decays to a W boson pair, with at least one W boson off-shell (WW*). These are the most likely and second-most likely Higgs boson decay channels, respectively. The otherwise large SM background of jets produced via quantum chromodynamics processes, referred to as "multijet" background, is greatly reduced by considering the WW* final state in which one W boson decays to quarks ($q\overline{q}'$) and the other to either an electron-neutrino pair ($e\nu$) or a muon-neutrino pair ($\mu\nu$). This search is optimized for particle mass $m_X > 0.8\,\text{TeV}$ and employs new techniques for this channel to recognize substructure within boosted jets. The search is performed on a data set collected in 2016 at the CERN LHC, corresponding to an integrated luminosity of $35.9\,\text{fb}^{-1}$ of proton-proton (pp) collisions at $\sqrt{s} = 13\,\text{TeV}$.

The Higgs bosons have a high Lorentz boost because of the large values of m_X considered, and the decay products of each one are produced in a collimated cone. The $H \to b\overline{b}$ decay is reconstructed as a single jet, referred to as the $b\overline{b}$ jet, with high transverse momentum p_T. The $H \to WW^*$ decay is also reconstructed as a single jet, referred to as the $q\overline{q}'$ jet, but with a nearby lepton (e or μ). In both cases, the jets are required to have a reconstructed topology consistent with a substructure arising from a boson decaying to two quarks. The semileptonic Higgs boson decay chain is reconstructed from both the visible decay products and the missing transverse momentum. A distinguishing characteristic of the signal is a peak in the two-dimensional plane of the $b\overline{b}$ jet mass $m_{b\overline{b}}$ and the reconstructed HH invariant mass m_{HH}.

The main SM background to this search arises from top quark pair $t\overline{t}$ production in which one top quark decays via a charged lepton ($t \to Wb \to \ell\nu b$) and the other decays exclusively to quarks ($t \to Wb \to q\overline{q}'b$). The top quarks affecting this analysis have decay products that are collimated because of large boosts. In particular, the all-hadronic top quark decays can be misreconstructed as single $b\overline{b}$ jets. Peaks in the $m_{b\overline{b}}$ distribution from this background correspond to fully contained top quark and W boson decays. The second-largest background is primarily composed of production of W bosons in association with jets (W+jets) and multijet events. Both W+jets and multijet background events are experimentally distinct from $t\overline{t}$ production, in part because their $m_{b\overline{b}}$ distributions are smoothly falling.

In this analysis, the events are divided into 12 exclusive categories by lepton flavor, $q\overline{q}'$ jet substructure, and $b\overline{b}$ jet flavor identification. The SM background and signal yields are then simultaneously estimated using a maximum likelihood fit to the two-dimensional distribution in the $m_{b\overline{b}}$ and m_{HH} mass plane.

2 The CMS detector

The central feature of the CMS apparatus is a superconducting solenoid of 6 m internal diameter, providing a magnetic field of 3.8 T. Within the solenoid volume are a silicon pixel

and strip tracker, a lead tungstate crystal electromagnetic calorimeter (ECAL), and a brass and scintillator hadron calorimeter (HCAL), each composed of a barrel and two endcap sections. Forward calorimeters extend the coverage in pseudorapidity η provided by the barrel and endcap detectors. Muons are detected in gas-ionization chambers embedded in the steel flux-return yoke outside the solenoid. Events of interest are selected using a two-tiered trigger system [58]. The first level, composed of custom hardware processors, uses information from the calorimeters and muon detectors to select events at a rate of around 100 kHz within a time interval of less than 4 μs. The second level, known as the high-level trigger, consists of a farm of processors running a version of the full event reconstruction software optimized for fast processing, and reduces the event rate to around 1 kHz before data storage. A more detailed description of the CMS detector, together with a definition of the coordinate system used and the relevant kinematic variables, can be found in ref. [59].

3 Simulated samples

Signal and background yields are extracted from data with a fit using templates of the two-dimensional $m_{b\overline{b}}$ and m_{HH} mass distribution. The signal and background templates are obtained from samples generated using Monte Carlo simulation.

The signal process pp $\to$ X $\to$ HH $\to$ b$\overline{b}$WW* is simulated for both the spin-0 and spin-2 resonance scenarios. The X bosons are produced via gluon fusion and have a 1 MeV resonance width, which is small compared to the experimental resolution. The samples are generated at leading order (LO) using the MADGRAPH5_AMC@NLO 2.2.2 generator [60] with MLM merging [61] for m_X between 0.8 and 3.5 TeV.

The background processes are produced with a variety of generators. The same generator as for signal is used to produce t$\overline{t}$, W+jets, multijet, Higgs boson production in association with a t quark (tH), and Drell-Yan samples. Samples of WZ diboson production and the associated production of t$\overline{t}$ with either a W or Z boson (t$\overline{t}$ + V) are also generated with MADGRAPH5_AMC@NLO, but at next-to-leading-order (NLO) with the FxFx jet merging scheme [62]. The WW diboson process, single top production, and t$\overline{t}$H are generated with POWHEG v2 at NLO [63–70]. Single top in the associated production (tW) and t-channel (tq) processes are included, but not s-channel (tb), which is negligible.

For all samples, the parton showering and hadronization are simulated with PYTHIA 8.205 [71] using the CUETP8M1 [72] tune, with NNPDF 3.0 [73] parton distribution functions (PDFs). The simulation of the CMS detector is performed with the GEANT4 [74] toolkit. Additional pp collisions in the same or nearby bunch crossings (pileup) are simulated and the samples are weighted to have the same pileup multiplicity as measured in data.

While the final background normalizations are extracted from data with the template fit, all processes are initially normalized to their theoretical cross sections, using the highest order available. The t$\overline{t}$ process is rescaled to the next-to-next-to-leading-order (NNLO) cross section, computed with TOP++ v2.0 [75]. The W+jets and Drell-Yan samples are also normalized using NNLO cross sections, but calculated with FEWZ v3.1 [76]. NLO cross sections are used for the single top and diboson samples, calculated with MCFM v6.6. [77–

79]. The multijet and $t\bar{t} + V$ cross sections are obtained from MadGraph5_aMC@nlo at LO and NLO accuracy, respectively. NLO cross sections are used for the $t\bar{t}H$ and tH processes [80].

4 Event reconstruction

Signal events and those from the primary SM background source, $t\bar{t}$ production with a single-lepton final state, have similar signatures. Both processes feature high-p_T jets with substructure consistent with two or more quarks, jets containing b hadron decays, and leptons that originate from a W boson decay. Additional discrimination of signal events from background events is achieved by associating the lepton and each jet with a particle in the $HH \to b\bar{b}WW^* \to b\bar{b}\ell\nu q\bar{q}'$ decay chain and applying mass constraints.

A particle-flow (PF) algorithm [81] aims to reconstruct and identify each individual particle in an event, with an optimized combination of information from the various elements of the CMS detector. The reconstructed vertex with the largest value of summed tracking-object p_T^2 is taken to be the primary pp interaction vertex. These tracking objects are track jets and the negative vector sum of the track jet p_T. Track jets are clustered using the anti-k_T jet finding algorithm [82, 83] with the tracks assigned to the vertex as inputs.

4.1 Electron and muon identification

Events are required to have exactly one isolated lepton. This lepton is associated with the leptonic W boson decay. Reconstructed electrons are required to have $p_T > 20\,\text{GeV}$ and $|\eta| < 2.5$, and are identified with a high-purity selection to suppress the potentially large multijet background [84]. Muons are required to have $p_T > 20\,\text{GeV}$ and $|\eta| < 2.4$, and to pass identification criteria optimized to select muons with $>95\%$ efficiency [85]. The impact parameter of lepton tracks with respect to the primary vertex is required to be consistent with originating from that vertex: longitudinal distance $<0.1\,\text{cm}$, transverse distance $<0.05\,\text{cm}$, and significance <4 standard deviations of the three-dimensional displacement. These criteria remove background events where the lepton is produced by a semileptonic heavy-flavor decay rather than a W boson decay. In addition, these criteria prevent incorrectly selecting a lepton from a heavy-flavor decay in signal events. Requiring leptons to be isolated from nearby hadronic activity is important to suppress background, but can also cause significant signal inefficiency because of the collinear decay of the Lorentz-boosted Higgs boson. This inefficiency is mitigated by using an isolation definition specifically designed for leptons from boosted decays [86]. The isolation metric I_{rel} is the p_T sum of the PF particles with $\Delta R < \Delta R_{\text{iso}}$ with respect to the lepton, divided by the lepton p_T. The angular distance is $\Delta R = \sqrt{(\Delta\eta)^2 + (\Delta\phi)^2}$. The value ΔR_{iso} is defined to be

$$\Delta R_{\text{iso}} = \begin{cases} 0.2, & p_T < 50\,\text{GeV}, \\ 10\,\text{GeV}/p_T, & 50 < p_T < 200\,\text{GeV}, \\ 0.05, & p_T > 200\,\text{GeV}, \end{cases} \qquad (4.1)$$

which preserves signal efficiency even in the case of high m_X. The neutral particle contribution to I_{rel} from pileup interactions is estimated and removed using the method described in ref. [84]. Electrons are selected with $I_{rel} < 0.1$, whereas muons, because of lower background rates, are selected with $I_{rel} < 0.2$.

Muons in signal events have an approximate efficiency of 85% for $m_X = 0.8\,\text{TeV}$, decreasing to 70% for $m_X = 3.5\,\text{TeV}$, with isolation being the leading source of inefficiency compared to all other requirements. The efficiency to select electrons is lower, approximately 40% for $m_X = 0.8\,\text{TeV}$, decreasing to 6% for $m_X = 3.5\,\text{TeV}$. The leading source of electron inefficiency is a selection imposed at the reconstruction level on the ratio of the energy deposited in the HCAL to that deposited in the ECAL. Signal electrons typically fail this selection because of the nearby energy deposits from the hadronic W boson decay. Lepton reconstruction, identification, and isolation efficiencies are measured in a $Z \rightarrow \ell\ell$ data sample with a "tag-and-probe" method [87] and the simulation is corrected for any discrepancies with the data. There is generally much less hadronic activity in $Z \rightarrow \ell\ell$ events than in signal events, so these corrections are parameterized by nearby hadronic activity to ensure their applicability. For this measurement, a lepton's hadronic activity is quantified by using the PF particles with $\Delta R < 0.4$ about the lepton to obtain two variables: the relative p_T sum around the lepton and the ΔR between the lepton and the $\vec{p}$ sum of these particles. When parameterized by these two variables, a similar drop in efficiency is measured in low ΔR and high relative momentum $Z \rightarrow \ell\ell$ events as in signal events. The lepton selection efficiencies in simulation are found to be within 10% of those in data. The uncertainty in the correction is at its largest for high hadronic activity, with a maximum value of 10% for electrons and 5% for muons.

4.2 Jet clustering and momentum corrections

Two types of jets are used. Because the X bosons being considered here are much more massive compared to the mass of the Higgs bosons they decay into, the subsequent $H \rightarrow b\bar{b}$ and $W \rightarrow q\bar{q}'$ decays are each reconstructed as single, merged jets. These jets are formed by clustering PF particles according to the anti-k_T algorithm [82, 83] with a distance parameter of 0.8, and are referred to as AK8 jets. The PF particle or particles associated with the lepton are not included in the clustering of this jet type in order to prevent the $q\bar{q}'$ jet from containing the lepton's momentum. Jets of the second type, referred to as AK4 jets, are used to suppress background events from $t\bar{t}$ production by identifying additional jets originating from b quarks. These jets are also clustered according to the anti-k_T algorithm, but with a distance parameter of 0.4. Jets of both types are required to have $|\eta| < 2.4$ so that a majority of their area is within acceptance of the tracker. The AK8 jets are required to have $p_T > 50\,\text{GeV}$, whereas the threshold is $20\,\text{GeV}$ for AK4 jets.

Jet momentum for both jet types is determined as the vectorial sum of all particle momenta in the jet, and is found from simulation to be, on average, within 5 to 10% of the true momentum over the whole p_T spectrum and detector acceptance. Additional pp interactions within the same or nearby bunch crossings can contribute additional tracks and calorimetric energy depositions, increasing the apparent jet momentum. The pileup per particle identification (PUPPI) algorithm [88] is used to mitigate the effect of pileup

at the reconstructed particle-level, making use of local shape information, event pileup properties, and tracking information. Charged particles identified to be originating from pileup vertices are discarded. For each neutral particle, a local shape variable is computed using the surrounding charged particles compatible with the primary vertex within the tracker acceptance ($|\eta| < 2.5$), and using both charged and neutral particles in the region outside of the tracker coverage. The momenta of the neutral particles are then rescaled according to their probability to originate from the primary interaction vertex deduced from the local shape variable [89]. Jet energy corrections are derived from simulation studies so that the average measured response of jets becomes identical to that of particle level jets. In situ measurements of the momentum balance in dijet, photon+jet, Z+jet, and multijet events are used to determine any residual differences between the jet energy scale in data and in simulation, and appropriate corrections are made [90]. Additional selection criteria are applied to each jet to remove jets potentially dominated by instrumental effects or reconstruction failures [89].

4.3 Hadronic boson decay reconstruction

In high-m_X signal events, the $H \to WW^*$ decay is reconstructed as an AK8 jet and a nearby lepton, with the jet itself containing two localized energy deposits, "subjets", one from each quark. Only the AK8 jet closest in ΔR to the lepton is considered for $q\overline{q}'$ jet reconstruction. This jet satisfies $q\overline{q}'$ jet reconstruction criteria if it is close to the lepton ($\Delta R < 1.2$) and if two subjets with $p_T > 20\,\text{GeV}$ and $|\eta| < 2.4$ can be identified. The constituents of the jet are first reclustered using the Cambridge-Aachen algorithm [91, 92]. The "modified mass drop tagger" algorithm [93, 94], also known as the "soft drop" (SD) algorithm, with angular exponent $\beta = 0$, soft cutoff threshold $z_{\text{cut}} < 0.1$, and characteristic radius $R_0 = 0.8$ [95], is applied to remove soft, wide-angle radiation from the jet. The subjets used in the analysis are those remaining after the algorithm has removed all recognized soft radiation. The purity of the $q\overline{q}'$ jet reconstruction is quantified using the "N-subjettiness" variables τ_N, which measure compatibility with the hypothesis that a jet originates from N subjets [96]. The τ_N are obtained by first reclustering the jet into N subjets using the k_T algorithm [97]. The variables are then calculated with these subjets as described in ref. [96] with a characteristic radius $R_0 = 0.8$. The ratio of N-subjettiness variables, τ_2/τ_1, is used to discriminate $q\overline{q}'$ jets originating from two-pronged W boson decays against those from single quarks or gluons.

Generally, the Higgs bosons in signal events have large Lorentz boosts and are produced with $\Delta\phi \approx \pi$ between them. Therefore, $b\overline{b}$ jet candidates are required to be AK8 jets with $\Delta\phi > 2$ from the lepton and $\Delta R > 1.6$ from the $q\overline{q}'$ jet. If there are two or more $b\overline{b}$ jet candidates, the one leading in p_T is used. This jet is reconstructed as a $b\overline{b}$ jet if it is the leading or second-leading AK8 jet in p_T, has $p_T > 200\,\text{GeV}$, and if two constituent subjets with $p_T > 20\,\text{GeV}$ and $|\eta| < 2.4$ can be identified. The $b\overline{b}$ jet SD mass, which is the invariant mass of the two subjets, is used to obtain $m_{b\overline{b}}$. The mass grooming helps reject events for which the $b\overline{b}$ jet originates from a single quark or gluon. The performance of the SD algorithm varies with $b\overline{b}$ jet p_T, so simulation-derived $m_{b\overline{b}}$ correction factors are

applied as a function of p_T to make the average $m_{b\overline{b}}$ value be 125 GeV, the Higgs boson mass m_H [98].

4.4 Jet flavor identification

Jets and subjets are identified as likely to have originated from b hadron decays using the combined secondary vertex b tagging algorithm [99]. Two operating points of the algorithm are used, which have similar performance on subjets and AK4 jets. A high-efficiency working point, referred to as "loose", has an efficiency of $\approx$80% and a light-quark or gluon misidentification rate of $\approx$10%. The "medium" operating point has an efficiency and misidentification rate of $\approx$60% and $\approx$1%, respectively. A "tight" operating point is not used. Jets or subjets with $p_T > 30$ GeV and $|\eta| < 2.4$ are considered for b tagging. This lower bound on p_T is chosen because the uncertainty in b tagging calibrations is larger for lower p_T jets and because the b quarks in our signal events have large p_T. The b tagging efficiency and misidentification rate are measured in data, and the simulation is corrected for any discrepancy [99].

4.5 Semileptonic Higgs boson decay and signal mass reconstruction

The missing transverse momentum vector $\vec{p}_T^{\,\mathrm{miss}}$ is computed as the negative vector p_T sum of all the PF candidates in an event [100]. The $\vec{p}_T^{\,\mathrm{miss}}$ is modified to account for corrections to the energy scale of the reconstructed jets in the event. The $\vec{p}_T^{\,\mathrm{miss}}$ is an estimate of the transverse momentum of the neutrino in the semileptonic Higgs boson decay chain. The longitudinal momentum p_z of this neutrino is estimated by setting the invariant mass of the neutrino, the lepton, and the $q\overline{q}'$ jet to m_H and solving the corresponding second-order equation. If two real solutions exist, the one with the smaller magnitude is chosen. If the p_z solution is complex, the real component of the solution is used. Other methods for determining the neutrino p_z, including choosing the other p_z solution or incorporating the imaginary components, do not improve the m_{HH} resolution. The reconstructed momentum of the W boson that decays to leptons, referred to as the $\ell\nu$ candidate, is obtained from the lepton and the estimated neutrino momenta. The WW^* candidate momentum is then obtained from the combined $\ell\nu$ candidate and the $q\overline{q}'$ jet momenta. The invariant mass of this object and the $b\overline{b}$ jet is m_{HH}.

5 Event selection and categorization

Events are included in this search if they pass the following criteria that indicate they originate from a X boson decay and are then divided into 12 independent categories. A separate set of criteria is used to define control regions, which are used to validate the modeling of background processes.

5.1 Event selection

Events are selected by the trigger system if they contain one of the following: an isolated electron with $p_T > 27$ GeV, an isolated muon with $p_T > 24$ GeV, or $H_T > 800$ GeV (900 GeV for the last quarter of data taking), where H_T is the scalar sum of jet p_T for all AK4 online jets with $p_T > 30$ GeV. A combination (inclusive OR) of lepton and H_T triggers is

used because the online lepton isolation selection is inefficient for high-m_X signal, which provides two high-p_T, collimated Higgs boson decays. These events have large H_T and are instead selected with higher efficiency by the H_T trigger. Additional multi-object triggers that select events with a single lepton and $H_T > 400\,\text{GeV}$ supplement these two single-object triggers, thereby maintaining high signal trigger efficiency for the entire m_X analysis range. The pileup correction for H_T is the same offline as in the trigger. The trigger efficiency is measured for $\text{t}\bar{\text{t}}$ events in data and is >94% for events passing H_T and lepton p_T offline selection criteria. The simulation is corrected so that its trigger efficiency matches the efficiency measured with data. The trigger efficiency for signal events is 98% for $m_X = 0.8\,\text{TeV}$ and >99% for $m_X > 1\,\text{TeV}$.

Offline, events are required to have $H_T > 400\,\text{GeV}$ and a lepton with $p_T > 30\,\text{GeV}$ for electrons and $p_T > 26\,\text{GeV}$ for muons. Background events from $\text{Z} \to \ell\ell$ are suppressed by rejecting events that contain additional leptons with $p_T > 20\,\text{GeV}$. Events are further required to have a $\text{q}\bar{\text{q}}'$ jet and a $\text{b}\bar{\text{b}}$ jet. Background from $\text{t}\bar{\text{t}}$ production is reduced by vetoing events with AK4 jets that are $\Delta R > 1.2$ from the $\text{b}\bar{\text{b}}$ jet and pass the medium b tagging operating point.

Jets in multijet and $\text{W}+\text{jets}$ events tend to be produced at higher $|\eta|$ than those produced in signal events, which contain jets from the decay of a heavy resonance. The ratio p_T/m, which is the WW^* candidate p_T divided by m_{HH}, exploits this property and is especially effective at high m_{HH}. Events are required to have $p_T/m > 0.3$. A m_H constraint on the WW^* candidate is not useful because it is already imposed in the neutrino momentum calculation. However, there is discrimination because the decay chain involves a two-body decay as an intermediate step. We define a variable $m_D \equiv p_T \Delta R / 2$, where ΔR is the separation of the two reconstructed W bosons and the p_T is that of the WW^* candidate. This variable is based on an approximate expression for the opening angle of a highly boosted, massive particle decay. The selection $m_D < 125\,\text{GeV}$ is applied and has a high efficiency for signal events. The m_D and p_T/m distributions are shown in figure 1. This figure is shown only to illustrate how these variables are used to discriminate signal events from background events; the simulated distributions are pre-modeling and pre-fit. The initial difference in $m_{\text{b}\bar{\text{b}}}$ near $50\,\text{GeV}$ between simulation and data is apparent only with the pre-fit background model; with the full post-fit background model no discrepancy appears.

5.2 Event categorization

Events are categorized by event properties that reflect the signal purity. The categorization allows for a single set of selections that targets the full m_X range, which is preferable to search categories that are optimized for different mass ranges. Electron and muon events are separated because their efficiencies for background and signal are different, resulting in different signal purities. The electron and muon categories are labeled "e" and "μ", respectively, in the figures. There are three categories of b tagging, evaluated by counting the number of subjets in the $\text{b}\bar{\text{b}}$ jet that pass b tagging operating points. The first, labeled "bL", is composed of events in which one subjet passes the medium operating point and the other does not pass the loose operating point. Events with one subjet passing the medium
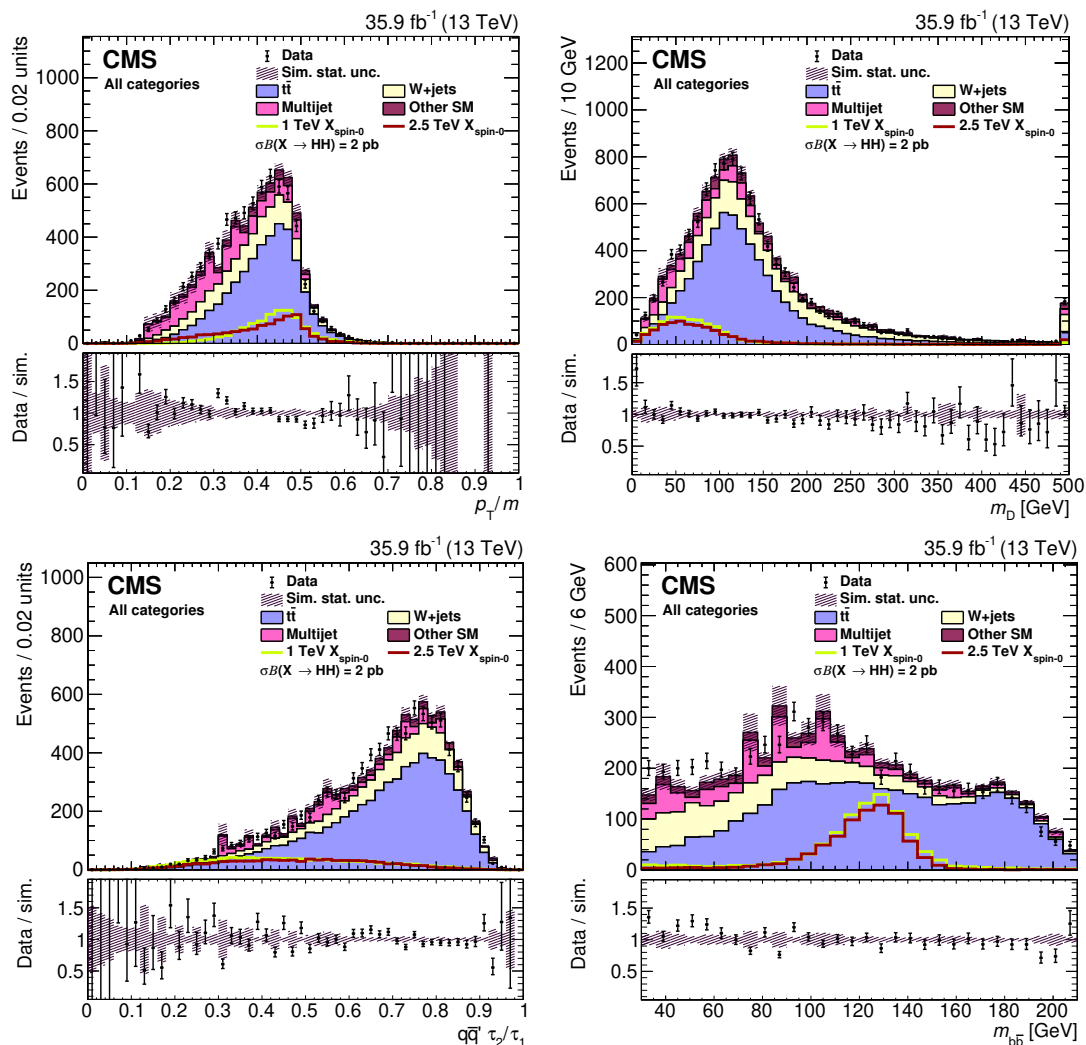
Figure 1. Pre-modeling and pre-fit distributions of the discriminating variables, which are described in the text, are shown for data (points) and SM processes (filled histograms) as predicted directly from simulation. The statistical uncertainty of the simulated sample is shown as the hatched band. The solid lines correspond to spin-0 signals for m_X of 1 and 2.5 TeV. The product of the cross section and branching fraction to two Higgs bosons is set to 2 pb for both signal models. The lower panels show the ratio of the data to the sum of all background processes.

operating point and one passing the loose but not the medium operating point are denoted "bM", and those with two subjets passing the medium operating point are labeled "bT". The final categorization is based on the τ_2/τ_1 N-subjettiness ratio of the $q\overline{q}'$ jet, referred to as $q\overline{q}'$ τ_2/τ_1. Events with $0.55 < q\overline{q}'$ $\tau_2/\tau_1 < 0.75$ fall into the low-purity category, "LP", while those with $q\overline{q}'$ $\tau_2/\tau_1 < 0.55$ are included in a high-purity category, "HP". The $q\overline{q}'$ τ_2/τ_1 distribution is shown in figure 1. Events are divided into all combinations of categories for a total of 12 exclusive selections. When describing a single selection, the category label is a combination of those listed above. For example, the tightest b tagging category with a low-purity $q\overline{q}'$ τ_2/τ_1 selection in the electron channel is: "e, bT, LP". The categories and their corresponding labels are summarized in table 1.

Categorization type	Selection	Category label
Lepton flavor	Electron	e
	Muon	μ
$b\bar{b}$ jet subjet b tagging	One medium	bL
	One medium and one loose	bM
	Two medium	bT
$q\bar{q}'$ jet substructure	$0.55 < q\bar{q}'\ \tau_2/\tau_1 < 0.75$	LP
	$q\bar{q}'\ \tau_2/\tau_1 < 0.55$	HP

Table 1. Event categorization and corresponding category labels. All combinations of the two lepton flavor, three $b\bar{b}$ jet subjet b tagging, and two $q\bar{q}'$ jet substructure selections are used to form 12 independent event categories. For the $b\bar{b}$ jet subjet b tagging type, "medium" refers to the subjets that pass the medium b tagging operating point and "loose" refers to those that pass the loose, but not the medium, operating point.

The search is performed in these categories for $30 < m_{b\bar{b}} < 210\,\text{GeV}$. Events below $30\,\text{GeV}$ would provide little sensitivity and would be relatively difficult to model since these are events for which the SD algorithm results in nearly all of the jet energy being removed. The $m_{b\bar{b}}$ distribution is displayed in figure 1. Events with $700 < m_{\text{HH}} < 4000\,\text{GeV}$ are analyzed. The lower bound is chosen such that the m_{HH} distribution is monotonically decreasing for background events. The upper bound is far above the highest mass event observed in data. For spin-0 scenarios, the selection efficiency for $\text{X} \to b\bar{b}q\bar{q}'\ell\nu$ events to pass the criteria of any event category is 9% at $m_{\text{X}} = 0.8\,\text{TeV}$. The efficiency increases with m_{X} to 18% at $m_{\text{X}} = 1.2\,\text{TeV}$ because the Higgs boson decays become more collimated. Above $1.2\,\text{TeV}$ the selection efficiency decreases to a minimum of 9% at $m_{\text{X}} = 3.5\,\text{TeV}$ because of the combination of lower b tagging efficiency for high-p_{T} jets and the worsening of the lepton isolation for extremely collimated Higgs boson decays. The Higgs bosons in spin-2 signal events are more central in polar angle than those from spin-0 signal, resulting in a larger selection efficiency, $\approx$15%, relative.

5.3 Control region event selection and categorization

Two control regions are used to validate the SM background estimation and to obtain systematic uncertainties. The first, labeled "$t\bar{t}$ CR", targets backgrounds with top quarks, specifically $t\bar{t}$ production. Such events are selected by inverting the AK4 jet b-tagging veto. The m_{D} and p_{T}/m selections are removed to increase the statistical power of the sample. This control region is then divided into the 12 categories previously described. Overall, the $m_{b\bar{b}}$ and m_{HH} shapes in this control region are very similar to the shapes in the signal region for the backgrounds that contain top quarks. The top quark p_{T} spectrum in $t\bar{t}$ events has been shown to be mis-modelled in simulation [101, 102]. A correction is measured in this region and applied to the simulation as a normalization correction. However, ultimately the final value of the normalization and its uncertainty come from the two-dimensional fit to signal and background. While the $t\bar{t}$ CR is an adequate probe of processes that involve top quarks, it is not sensitive to the multijet or W+jets backgrounds.

Instead, a second control region, labeled "q/g CR", is used to study the modeling of the mass shapes and the relative composition of the W + jets and the multijet backgrounds, which is similar to their relative composition in the search region. The selection of events in this control region is the same as for the signal region, except that the $b\overline{b}$ jet is required to have no subjets passing the loose b tagging operating point. As a result, the events in this control region are not categorized by $b\overline{b}$ jet b tagging, but are still categorized by lepton flavor and $q\overline{q}'$ τ_2/τ_1.

6 Background and signal modeling

The search is performed by simultaneously estimating the signal and background yields using a maximum likelihood fit to the data in the 12 event categories. The data are binned in two dimensions, m_{HH} and $m_{b\overline{b}}$, with the ranges specified in section 5 and with bin widths of 25 and 2 GeV, respectively. The bin widths are smaller than the mass resolutions, but large enough to keep the number of bins computationally tractable. Each processes is modeled with two-dimensional templates, one for each event category. The templates are created using simulation. Because of the limited size of the simulated samples, we employ methods to smooth the background distributions. Shape uncertainties that account for possible differences between data and simulation are included while executing the fit. This fitting method was previously presented in ref. [52].

6.1 Background categorization

Background events are separated into four generator-level categories, each with distinct $m_{b\overline{b}}$ shapes. The categories are defined by counting the number of generator-level quarks from the immediate decay of a top quark, W boson, or (rarely) Z boson within $\Delta R < 0.8$ of the $b\overline{b}$ jet axis. The first, labeled "m_{t} background", is the component in which all three quarks from a single top quark decay fulfill this criterion. The second is labeled "m_{W} background" and consists of those events that are not labeled m_{t} background but in which both quarks from a W or Z boson fall within the jet cone. Both of these backgrounds contain resonant peaks in the $m_{b\overline{b}}$ shape corresponding to either the top quark or W boson mass. The "lost t/W background" contains events with partial decays within the $b\overline{b}$ jet, identified as events in which at least one quark is contained within the jet cone, but does not satisfy one of the previous two requirements. The last category, "q/g background", designates all other events. The first three categories are primarily composed of $t\overline{t}$ events, while the last is a composite of W + jets, multijet, and $t\overline{t}$ events. The background categorization is summarized in table 2.

6.2 Template creation strategy

A template is produced for each of the 12 event categories, for each of the four backgrounds. To reduce statistical fluctuations in the templates, each is generated from an initial smooth template created by relaxing requirements or by combining categories. In all cases, the regions with relaxed criteria are chosen such that the shapes for these regions are similar to those for the full event selection. The final template for each event category

Bkg. category	Dominant SM process(es)	Resonant in $m_{b\overline{b}}$	Num. of gen.–level quarks
m_t	$t\overline{t}$	Yes (near m_t)	3 from t
m_W	$t\overline{t}$	Yes (near m_W)	2 from W
Lost t/W	$t\overline{t}$	No	1 or 2
q/g	W+jets and multijet	No	0

Table 2. The four exclusive background categories with their kinematical properties and defining number of generator-level quarks within $\Delta R < 0.8$ of the $b\overline{b}$ jet axis.

and background is produced by fitting the high-statistics template to the simulated samples for that category's event selection. The fit is performed in a similar manner to the fit to data and with a similar parameterization of the template shape. The templates are compared to simulation after applying the full event selection and any deviations in shape are found to be much smaller than the statistical uncertainty of the data sample. The background templates and associated systematic uncertainties are ultimately validated by fitting to data in dedicated control regions, which is described in section 6.5.

While this procedure increases the statistical power of the simulation samples, the multijet background simulation sample cannot be produced with a large enough effective integrated luminosity to be directly used in the template creation. Instead, the similarity of $m_{b\overline{b}}$ reconstruction for W+jets and multijet events is exploited. Both these processes have $b\overline{b}$ jets that are composed of at least one quark or gluon that is misidentified as a $b\overline{b}$ jet, resulting in nearly identical monotonically falling $m_{b\overline{b}}$ shapes. Both processes also have similar relative fractions in the bL, bM, and bT categories. The W+jets and multijet samples are used to obtain a combined yield and m_{HH} distribution for each lepton flavor and $q\overline{q}'$ τ_2/τ_1 category. The $m_{b\overline{b}}$ modeling and the relative $b\overline{b}$ jet subjet b tagging categorization is then taken from the W+jets sample. These two components are combined to form a single background shape when forming the q/g background templates.

6.3 Background process modeling

The background templates are modeled as conditional probabilities of $m_{b\overline{b}}$ as a function of m_{HH} so that the templates include the correlation of these two variables. The two-dimensional probability distribution is

$$P_{\text{bkg}}(m_{b\overline{b}}, m_{HH}) = P_{b\overline{b}}(m_{b\overline{b}}|m_{HH}, \theta_1)P_{HH}(m_{HH}|\theta_2), \tag{6.1}$$

where P_{HH} and $P_{b\overline{b}}$ are one-dimensional probability distributions and the θ_1 and θ_2 are nuisance parameters used to account for shape uncertainties. A parametric function that models the full m_{HH} range for background events is difficult to obtain from first principles. Instead, a non-parametric approach is taken. The P_{HH} are produced from the one-dimensional m_{HH} histograms with kernel density estimation (KDE) [103–105]. The smoothing of the P_{HH} distributions is controlled by parameters within the KDE framework called bandwidths. Gaussian kernels with adaptive bandwidths are used because the event density for this distribution varies strongly with m_{HH} and a single, global bandwidth

is not suitable for the full distribution. These adaptive bandwidths depend on a first iteration estimate of P_{HH}, which itself is produced with KDE. However, for this first iteration a global bandwidth h is used that scales as

$$h \propto \left(\frac{\left(\sum_{i=1}^{n} w_i \right)^2}{\sum_{i=1}^{n} w_i^2} \right)^{-1/5}. \tag{6.2}$$

The sums are over all events in the simulation sample and the w_i are the individual event weights. This formulation is chosen to minimize the mean integrated squared error of the estimate. For the adaptive estimates, the bandwidths h_i associated with each event are

$$h_i = h \left(\frac{g}{\widetilde{f}(x_i)} \right)^{1/2}, \tag{6.3}$$

where the $\widetilde{f}(x_i)$ are the estimated event densities at the location x_i of the event and g is a normalization factor such that the global bandwidth scale is controlled by h. As discussed in ref. [106], adaptive KDE can result in overestimation of the distribution tails in the case of large bandwidths being applied. This is ameliorated by imposing a maximum bandwidth value, which is usually chosen to be 1–5 times larger than the median bandwidth. The m_{HH} tail is further smoothed by fitting with an exponential function for $m_{\mathrm{HH}} \gtrsim 2\,\mathrm{TeV}$.

The $P_{\mathrm{b\overline{b}}}$ distributions are obtained for the m_{t} and m_{W} backgrounds by fitting $m_{\mathrm{b\overline{b}}}$ histograms with a double Crystal Ball function [107, 108]. This function has a Gaussian core, which is used to model the bulk of the $m_{\mathrm{b\overline{b}}}$ distribution, and power-law tails, which describe the effects of more severe jet misreconstruction. The fits are performed for events binned in m_{HH} to capture the evolution of the $m_{\mathrm{b\overline{b}}}$ shape with m_{HH}. The double Crystal Ball function parameters are then interpolated between m_{HH} bins. The $P_{\mathrm{b\overline{b}}}$ distributions for the lost t/W and q/g backgrounds are estimated from the two-dimensional histograms with two-dimensional KDE. Independent adaptive bandwidths and bandwidth upper limits are used for each dimension when forming the $P_{\mathrm{b\overline{b}}}$. Similar to the derivation of the P_{HH}, the m_{HH} tails are smoothed with exponential function fits. Simulation yields are used as the initial values of the background yields in the fit to data.

6.4 Signal process modeling

The signal templates are also modeled as conditional probabilities

$$P_{\mathrm{signal}}(m_{\mathrm{b\overline{b}}}, m_{\mathrm{HH}}|m_{\mathrm{X}}) = P_{\mathrm{HH}}(m_{\mathrm{HH}}|m_{\mathrm{b\overline{b}}}, m_{\mathrm{X}}, \theta_1) P_{\mathrm{b\overline{b}}}(m_{\mathrm{b\overline{b}}}|m_{\mathrm{X}}, \theta_2). \tag{6.4}$$

The P_{signal} distributions are first obtained for discrete m_{X} values by fitting histograms of the signal mass distributions. Models continuous in m_{X} are then produced by interpolating the fit parameters. The $P_{\mathrm{b\overline{b}}}$ distributions are created by fitting $m_{\mathrm{b\overline{b}}}$ histograms with a double Crystal Ball function, and the resonance resolution is $\approx 10\%$. The shape for the bL categories also includes an exponential function to model the small fraction of signal events with no resonant peak in the distribution.

The P_{HH} distributions are also modeled with a double Crystal Ball function, but with a linear dependence on $m_{\mathrm{b\overline{b}}}$, parameterized by $\Delta_{\mathrm{b\overline{b}}} = (m_{\mathrm{b\overline{b}}} - \mu_{\mathrm{b\overline{b}}})/\sigma_{\mathrm{b\overline{b}}}$. The $\mu_{\mathrm{b\overline{b}}}$ and $\sigma_{\mathrm{b\overline{b}}}$

are the mean and standard deviation parameters from the fit to $m_{b\overline{b}}$, respectively. The variable μ_{HH}, the mean of the Crystal Ball function, is then

$$\mu_{HH} = \mu_0(1 + \mu_1\Delta_{b\overline{b}}),$$ (6.5)

where μ_0 and μ_1 are fit parameters. This parameterization models the characteristic that a mismeasurement of the $b\overline{b}$ jet results in a mismeasurement of m_{HH}. The standard deviation of m_{HH}, denoted as σ_{HH}, also depends on $m_{b\overline{b}}$,

$$\sigma_{HH} = \begin{cases} \sigma_0(1 + \sigma_1|\Delta_{b\overline{b}}|), & \Delta_{b\overline{b}} < 0, \\ \sigma_0, & \Delta_{b\overline{b}} > 0, \end{cases}$$ (6.6)

where σ_0 and σ_1 are fit parameters. An undermeasurement of $m_{b\overline{b}}$ can be caused by the SD algorithm removing energy from the Higgs boson decay. In such a scenario, the correlation between the two variables worsens and the m_{HH} resolution becomes wider. For $|\Delta_{b\overline{b}}| > 2.5$, only the values at the boundary are used since the correlation does not hold for severe mismeasurements. The m_{HH} resolution is $\approx$6% for $m_X = 1\,\mathrm{TeV}$, decreasing to 4% for $m_X = 3\,\mathrm{TeV}$.

The product of the acceptance and efficiency for $X \to HH$ events to be included in the individual event categories is taken from simulation. As for the shape parameters, the efficiency is interpolated in m_X. Uncertainties in the relative acceptances and in the integrated luminosity of the sample are included in the maximum likelihood fit that is used to obtain confidence intervals on the $X \to HH$ process. The modeling is tested by fitting the templates to pseudo-experiments with injected signal and no significant bias in the fitted signal yield is found.

6.5 Validation of background models with control region data

The background models are validated by analyzing the $t\overline{t}$ CR and q/g CR data samples. For both control regions, background templates are constructed in the same way as for the standard event selection, except that they are made to model the control region selection. The background templates are then fit to the control region data with the same systematic uncertainties that are used in the standard maximum likelihood fit. The result of the simultaneous fit is shown in figure 2 for both control regions. To improve visualization, the displayed binning shown in this and subsequent figures is coarser than that used in the maximum likelihood fit. The projections in both mass dimensions are shown for the combination of all event categories. The fit result models the data well, indicating that the shape uncertainties can account sufficiently for potential differences between data and simulation.

7 Systematic uncertainties

Systematic uncertainties are included in the maximum likelihood fit as nuisance parameters. Nuisance parameters for shape uncertainties are modeled as Gaussian functions, whereas log-normal functions are used for normalization uncertainties. The $m_{b\overline{b}}$ scale and
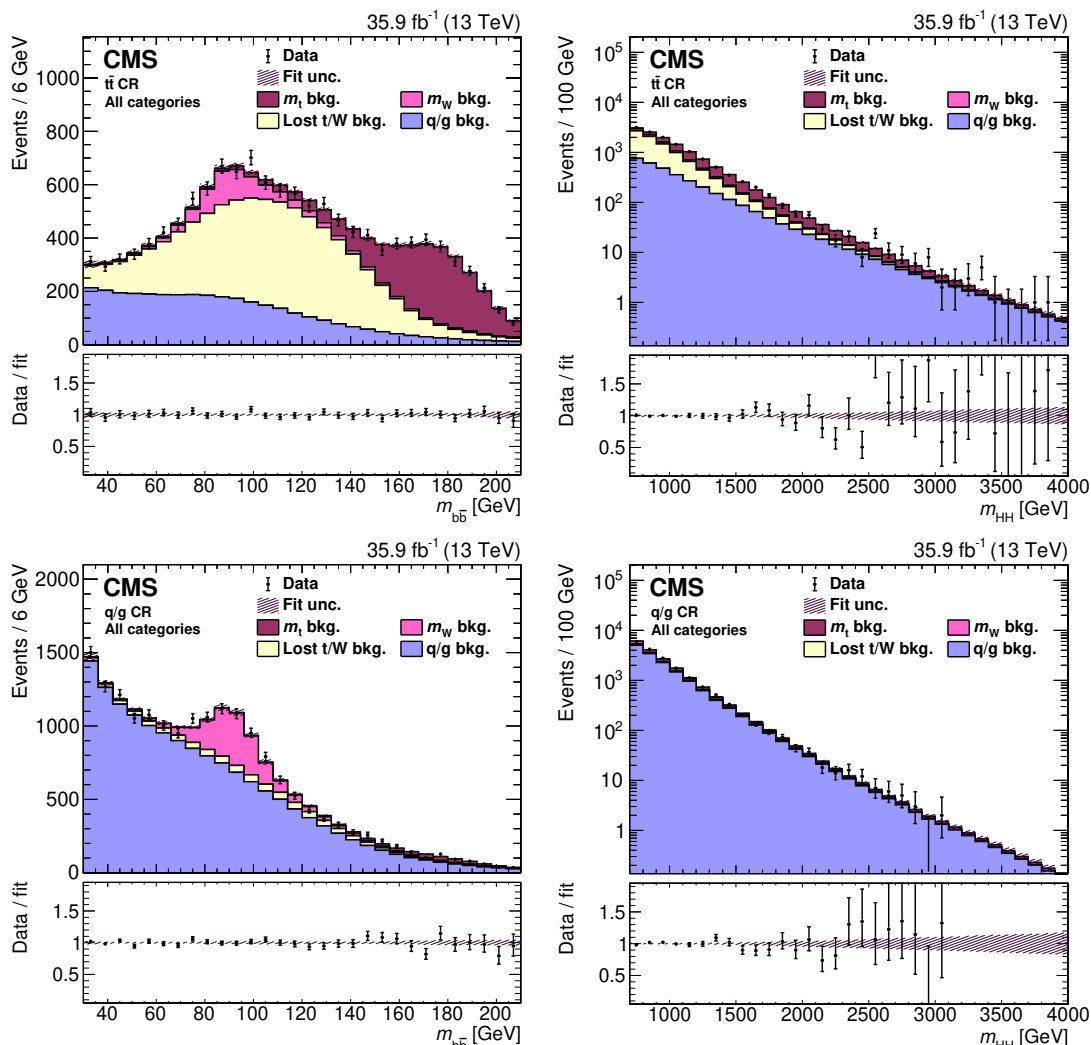
Figure 2. The fit result compared to data in the $t\bar{t}$ CR (upper plots) and q/g CR (lower plots), projected in $m_{b\bar{b}}$ (left) and m_{HH} (right). Events from all categories are combined. The fit result is the filled histogram, with the different colors indicating different background categories. The background shape uncertainty is shown as the hatched band. The lower panels show the ratio of the data to the fit result.

resolution uncertainties for the signal, the m_t background, and the m_W background are evaluated as uncertainties in the mean and standard deviation of the double Crystal Ball function parameters, respectively. The signal m_{HH} scale and resolution uncertainties are handled in the same manner. The other background shape uncertainties are implemented as alternative background templates. Each alternative template is produced by shifting the nominal background template, bin-by-bin, by a factor that depends on either m_{HH} or $m_{b\bar{b}}$. The magnitudes of these factors are subsequently constrained as nuisance parameters.

The parameterization of the background uncertainties is motivated by the expectation of possible differences between simulation and data for such aspects as background composition or jet energy scale. Studies of the $t\bar{t}$ CR and the q/g CR are used to verify that the

chosen uncertainties do cover these differences. More complex background models, such as those with more nuisance parameters or higher order shape distortions, are also tested in these control regions. The more complex background models do not lead to better agreement between data and the fit result. The fit result does not depend strongly on the initial uncertainty sizes because they function only as loose constraints for the fit. This is verified by inflating all initial background uncertainty sizes by a factor of two and observing that the final result does not change. Therefore, the initial background uncertainty sizes are sufficiently large to easily account for the differences between simulation and data in the control regions.

Shape distortions derived from differences between simulation generator programs, parton showering and simulation programs, and matrix element calculation order were also studied. The uncertainties used in obtaining this result are comparable to or larger than those derived from these differences. Each uncertainty is listed in table 3 with its initial size. A single uncertainty type can be applied to multiple event categories with independent nuisance parameters per category. The background model includes 98 nuisance parameters, while the signal model includes 13 and shares an additional two with the background model. The description of each uncertainty, including correlations between event categories, is described in sections 7.1–7.3.

7.1 Background normalization uncertainties

Since the main source of the m_t, m_W, and lost t/W backgrounds is $t\bar{t}$ production, some uncertainties are applied by treating the three categories as a single component, referred to collectively as the "non-q/g background".

The fraction of each of the three categories within the combination is determined from the overall b tagging efficiency and the $b\bar{b}$ jet p_T distributions. Additional uncertainties are then assigned to the modeling of their relative composition.

For each event category, the q/g background and the non-q/g background each have a large initial normalization uncertainty that is uncorrelated among categories. The relative composition of the three $t\bar{t}$ backgrounds is controlled in two ways. First, the m_W and lost t/W backgrounds have independent normalization uncertainties per b tagging category. In both cases, the m_t background normalization is varied in an anticorrelated manner such that the non-q/g background normalization does not change. Second, the composition is allowed to vary linearly with m_{HH} to account for $b\bar{b}$ jet reconstruction effects that depend on $b\bar{b}$ jet p_T. This is implemented with a m_{HH} shape uncertainty that only shifts the m_t background spectrum. There is one such independent nuisance parameter per b tagging category. Three other nuisance parameters shift the m_W and lost t/W backgrounds together.

7.2 Background shape uncertainties

The jet mass scale and resolution after applying the SD algorithm are measured for W boson decays merged into single jets in data with $t\bar{t}$ events, using the known W boson mass. The mass scale and resolution in the simulation are found to agree with the data within

Uncertainty label	Type	Processes	N_p	e_I	$e_\mathrm{C}/e_\mathrm{I}$
q/g normalization	Y	q/g	12	50%	27–48%
Non-q/g normalization	Y	m_t, m_W, lost t/W	12	25%	31–85%
Non-q/g categorization	Y	m_t, m_W, lost t/W	6	25%	12–99%
Non-q/g cat. p_T dep.	m_HH	m_t, m_W, lost t/W	6	$\pm 0.13(m_\mathrm{HH}/\,\mathrm{TeV})$	91–99%
SD scale	$m_\mathrm{b\overline{b}}$	m_t, m_W, signal	1	1%	52%
SD resolution	$m_\mathrm{b\overline{b}}$	m_t, m_W, signal	1	20%	31%
Lost t/W $m_\mathrm{b\overline{b}}$ scale	$m_\mathrm{b\overline{b}}$	Lost t/W	3	$\pm 0.0015(m_\mathrm{b\overline{b}}/\,\mathrm{GeV})$	91–99%
Lost t/W low $m_\mathrm{b\overline{b}}$	$m_\mathrm{b\overline{b}}$	Lost t/W	3	$\pm 18(\,\mathrm{GeV}/m_\mathrm{b\overline{b}})$	>87%
q/g $m_\mathrm{b\overline{b}}$ scale	$m_\mathrm{b\overline{b}}$	q/g	3	$\pm 0.0025(m_\mathrm{b\overline{b}}/\,\mathrm{GeV})$	90–96%
q/g low $m_\mathrm{b\overline{b}}$	$m_\mathrm{b\overline{b}}$	q/g	3	$\pm 30(\,\mathrm{GeV}/m_\mathrm{b\overline{b}})$	40–60%
Non-q/g m_HH scale	m_HH	m_t, m_W, lost t/W	12	$\pm 0.13(m_\mathrm{HH}/\,\mathrm{TeV})$	94–99%
Non-q/g m_HH resolution	m_HH	m_t, m_W, lost t/W	12	$\pm 0.28(\,\mathrm{TeV}/m_\mathrm{HH})$	95–99%
q/g m_HH scale	m_HH	q/g	12	$\pm 0.5(m_\mathrm{HH}/\,\mathrm{TeV})$	77–96%
q/g m_HH resolution	m_HH	q/g	12	$\pm 1.4(\,\mathrm{TeV}/m_\mathrm{HH})$	58–87%
Luminosity	Y	Signal	1	2.5%	—
PDF and scales	Y	Signal	1	2%	—
Trigger	Y	Signal	2	2%	—
Lepton selection	Y	Signal	2	e:5.7% μ:5.3%	—
Jet energy scale	Y, m_HH	Signal	1	Y:0.5% S:1% R:2%	—
Jet energy res.	Y, m_HH	Signal	1	Y:1% S:0.5% R:5%	—
Unclustered energy	Y, m_HH	Signal	1	Y:1% S:0.5% R:0.5%	—
b$\overline{b}$ jet b tagging	Y	Signal	1	<10%	—
AK4 jet b tagging veto	Y	Signal	1	1%	—
q$\overline{q}'$ τ_2/τ_1	Y	Signal	1	HP:14% LP:33%	—
q$\overline{q}'$ τ_2/τ_1 extrapolation	Y	Signal	1	<7%	—

Table 3. The systematic uncertainties included in the maximum likelihood fit and how they are applied to each process model. The "type" indicates if the uncertainty affects process yield Y or the shape of the $m_\mathrm{b\overline{b}}$ or m_HH distributions. Some uncertainties are applied to multiple event categories with independent nuisance parameters. The number of such parameters, N_p, the initial uncertainty size, e_I, and the ratios of the constrained size to the initial size, $e_\mathrm{C}/e_\mathrm{I}$, are listed. The ratios are obtained by fitting a model containing only background processes to the data. Uncertainty sizes that vary by event category are listed with category labels. The labels Y, S, and R denote how a single uncertainty affects yield, scale, and resolution, respectively.

uncertainties. These measurements determine the uncertainties in the $m_\mathrm{b\overline{b}}$ scale and resolution of the m_t and m_W backgrounds. For the lost t/W and q/g backgrounds, nuisance parameters are used to account for mismodeling of the simulated energy scale or the low-mass region by morphing the template shapes using a factor that is either proportional to, or inversely proportional to $m_\mathrm{b\overline{b}}$, respectively. The $m_\mathrm{b\overline{b}}$ shapes do not vary strongly with lepton flavor or q$\overline{q}'$ τ_2/τ_1, so a single pair of uncorrelated nuisance parameters is applied per background and b tagging category.

Mismodeling of the background p_T spectrum could manifest as an incorrect m_HH scale. This is accounted for by morphing the background templates by multiplicative

factors proportional to m_{HH}. Possible mismodeling of the m_{HH} resolution is considered in a similar manner, but with multiplicative factors proportional to m_{HH}^{-1}. A pair of scale and resolution uncertainties is assigned to the non-q/g background spectrum for each event category. An independent set of m_{HH} uncertainties for the q/g background is also included.

7.3 Signal uncertainties

A 2.5% uncertainty in the integrated luminosity [109] is included as a signal normalization uncertainty. Signal acceptance uncertainties from the choices of PDF, factorization scale, and renormalization scale are also applied. The scale uncertainties are obtained following the prescription found in refs. [110, 111], and the PDF uncertainty is evaluated using the NNPDF 3.0 PDF set [73]. Both the simulated trigger selection efficiency and the lepton selection efficiencies are corrected to match the data efficiencies. The uncertainties in these measurements are included as independent uncertainties in the electron and muon channel signal yields. Uncertainties in the jet energy scale, resolution, and unclustered energy resolution affect signal acceptance, m_{HH} scale, and m_{HH} resolution. The same $m_{b\overline{b}}$ scale and resolution uncertainties that are applied to the m_t and m_W backgrounds are applied to the signal. In this case, the background and signal uncertainties are 100% correlated.

The $b\overline{b}$ jet b tagging efficiency uncertainty is included as a single nuisance parameter that varies the signal normalization in each b tagging category. The uncertainty depends on m_X, with a maximum size of 10, 4, and 4% for the bT, bM, and bL categories, respectively. The bL category normalization uncertainty is anticorrelated with the other two uncertainties. A normalization uncertainty is assigned to the efficiency for passing the AK4 jet b tagging veto. The $q\overline{q}'$ τ_2/τ_1 selection efficiency is measured in a $t\overline{t}$ data sample for W bosons decaying to quarks. The uncertainty in this measurement is included as an uncertainty in the HP and LP category relative yields. An additional extrapolation uncertainty is applied because the jets in this sample have lower p_T than those in signal events. The uncertainty depends on m_X, with a maximum value of 7% for $m_X = 3.5\,\mathrm{TeV}$. The LP and HP selection efficiency uncertainties are anticorrelated.

8 Results

The data are interpreted by performing a maximum likelihood fit for a model containing only background processes and one containing both background and signal processes. The background-only fit is found to model the data. We interpret the results as upper limits on the product of the X production cross section and the X → HH branching fraction ($\sigma\mathcal{B}$).

The quality of the fit is quantified with the generalized χ^2 goodness-of-fit test using saturated models [112]. The probability distribution function of the test statistic is obtained with pseudo-experiments and the observed value is within the central 68% quantile of expected results. The best fit values of the nuisance parameters are consistent with the initial uncertainty ranges.

The fit result and the data are projected in $m_{b\overline{b}}$ for each event category in figures 3 and 4. The shape is modeled well, with each background category contributing to a specific subset of the mass range. In particular, the resonant peaks associated with W boson and
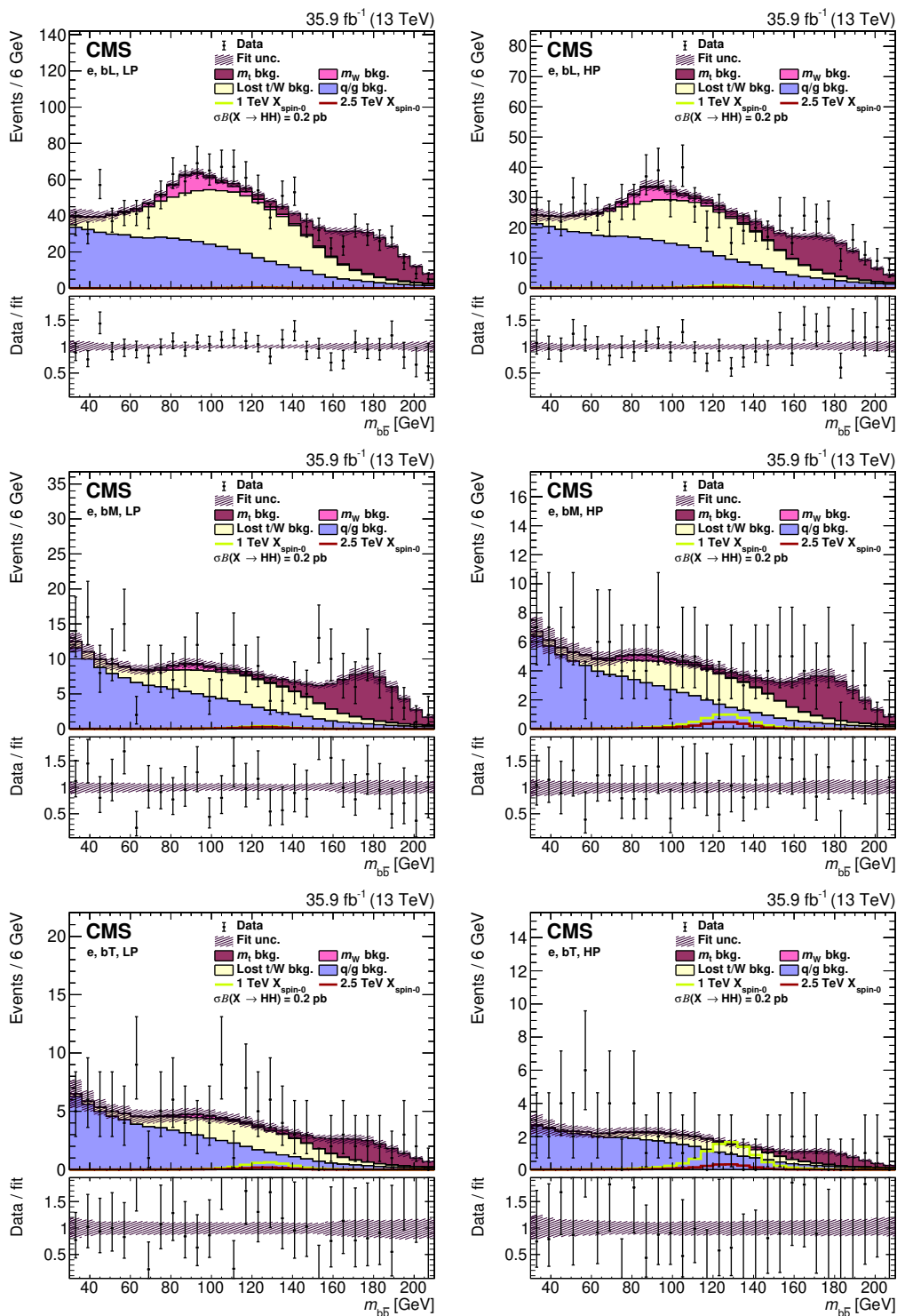
Figure 3. The fit result compared to data projected in $m_{b\overline{b}}$ for the electron event categories. The fit result is the filled histogram, with the different colors indicating different background categories. The background shape uncertainty is shown as the hatched band. Example spin-0 signal distributions for m_X of 1 and 2.5 TeV are shown as solid lines, with the product of the cross section and branching fraction to two Higgs bosons set to 0.2 pb. The lower panels show the ratio of the data to the fit result.
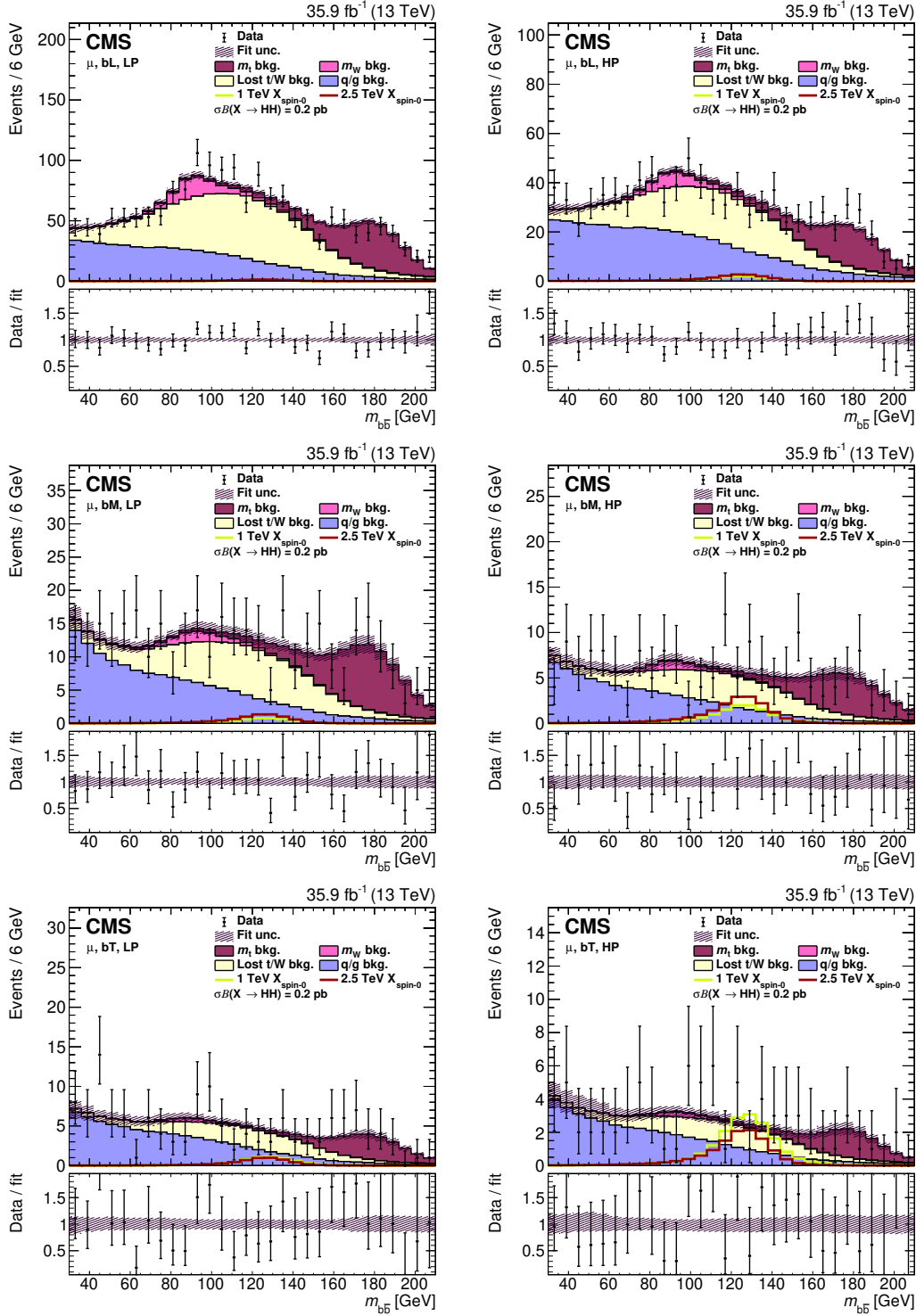
Figure 4. The fit result compared to data projected in $m_{b\bar{b}}$ for the muon event categories. The fit result is the filled histogram, with the different colors indicating different background categories. The background shape uncertainty is shown as the hatched band. Example spin-0 signal distributions for m_X of 1 and 2.5 TeV are shown as solid lines, with the product of the cross section and branching fraction to two Higgs bosons set to 0.2 pb. The lower panels show the ratio of the data to the fit result.

top quark decays are correctly modeled by the fit. Similarly, the projection in m_{HH} for each event category is shown in figures 5 and 6. Good agreement is found for the entire m_{HH} mass range.

The 95% confidence level (CL) upper limits are shown in figure 7 for varying m_{X} and both the spin-0 and spin-2 boson scenarios. The limits are evaluated using the asymptotic approximation [113] of the $\mathrm{CL_s}$ method [114, 115]. The observed exclusion limit is consistent with the expected limit; the most significant deviation between the two is about 1.5 standard deviations at $m_{\mathrm{X}} \approx 2.3\,\mathrm{TeV}$. The sources of the discrepancy are small excesses in data at high m_{HH} for the μ, bM, LP and μ, bL, HP event categories. The $m_{\mathrm{X}} = 0.8\,\mathrm{TeV}$ spin-0 signal is excluded for $\sigma\mathcal{B} > 123\,\mathrm{fb}$, with the exclusion limit strengthening to $\sigma\mathcal{B} > 8.3\,\mathrm{fb}$ for $m_{\mathrm{X}} = 3.5\,\mathrm{TeV}$ signal. The higher signal acceptance for spin-2 signal results in stronger constraints on $\sigma\mathcal{B}$: $>103\,\mathrm{fb}$ for $m_{\mathrm{X}} = 0.8\,\mathrm{TeV}$ signal and $>7.8\,\mathrm{fb}$ for $m_{\mathrm{X}} = 3.5\,\mathrm{TeV}$ signal. This search yields the best limits in this decay channel for $\mathrm{X} \to \mathrm{HH}$ production. It has similar sensitivity to resonances with $m_{\mathrm{X}} \approx 1\,\mathrm{TeV}$ to searches performed in other channels [50, 56]. This search is less sensitive to $m_{\mathrm{X}} \gtrsim 1.5\,\mathrm{TeV}$ resonances because of the degradation of the lepton selection efficiency for events with very large boost.

Predicted radion and bulk graviton cross sections [116] are also shown in figure 7 in the context of Randall-Sundrum models that allow the SM fields to propagate though the extra dimension. Typical model parameters are chosen as proposed in ref. [117]. For radions, a branching fraction of 25% to HH and an ultraviolet cutoff $\Lambda_R = 3\,\mathrm{TeV}$ are assumed. A 10% branching fraction is assumed for bulk gravitons, which occurs in scenarios that include significant coupling between the bulk graviton and top quarks. Bulk graviton production cross sections depend on the dimensionless quantity $\widetilde{k} = \sqrt{8\pi}k/M_{\mathrm{Pl}}$, where k is the curvature of the extra dimension and M_{Pl} is the Planck mass. For this interpretation, we choose $\widetilde{k} = 0.1$ and 0.3. For these particular signal parameters the radion and bulk graviton decay widths are larger than the 1 MeV width chosen for signal sample generation, but smaller than the detector resolution.

9 Summary

A search has been presented for new particles decaying to a pair of Higgs bosons (H) where one decays into a bottom quark pair ($\mathrm{b\overline{b}}$) and the other into two W bosons that subsequently decay into a lepton, a neutrino, and a quark pair. The large Lorentz boost of the Higgs bosons leads to the distinct experimental signature of one large-radius jet with substructure consistent with the decay $\mathrm{H} \to \mathrm{b\overline{b}}$ and a second large-radius jet with a nearby isolated lepton consistent with the decay $\mathrm{H} \to \mathrm{WW}^*$. This search uses a sample of proton-proton collisions collected at $\sqrt{s} = 13\,\mathrm{TeV}$ by the CMS detector, corresponding to an integrated luminosity of $35.9\,\mathrm{fb}^{-1}$. The primary standard model background, top quark pair production, is suppressed by reconstructing the HH decay chain and applying mass constraints. The signal and background yields are estimated by a two-dimensional template fit in the plane of the $\mathrm{b\overline{b}}$ jet mass and the HH resonance mass. The templates are validated in a variety of data control regions and are shown to model the data well. The
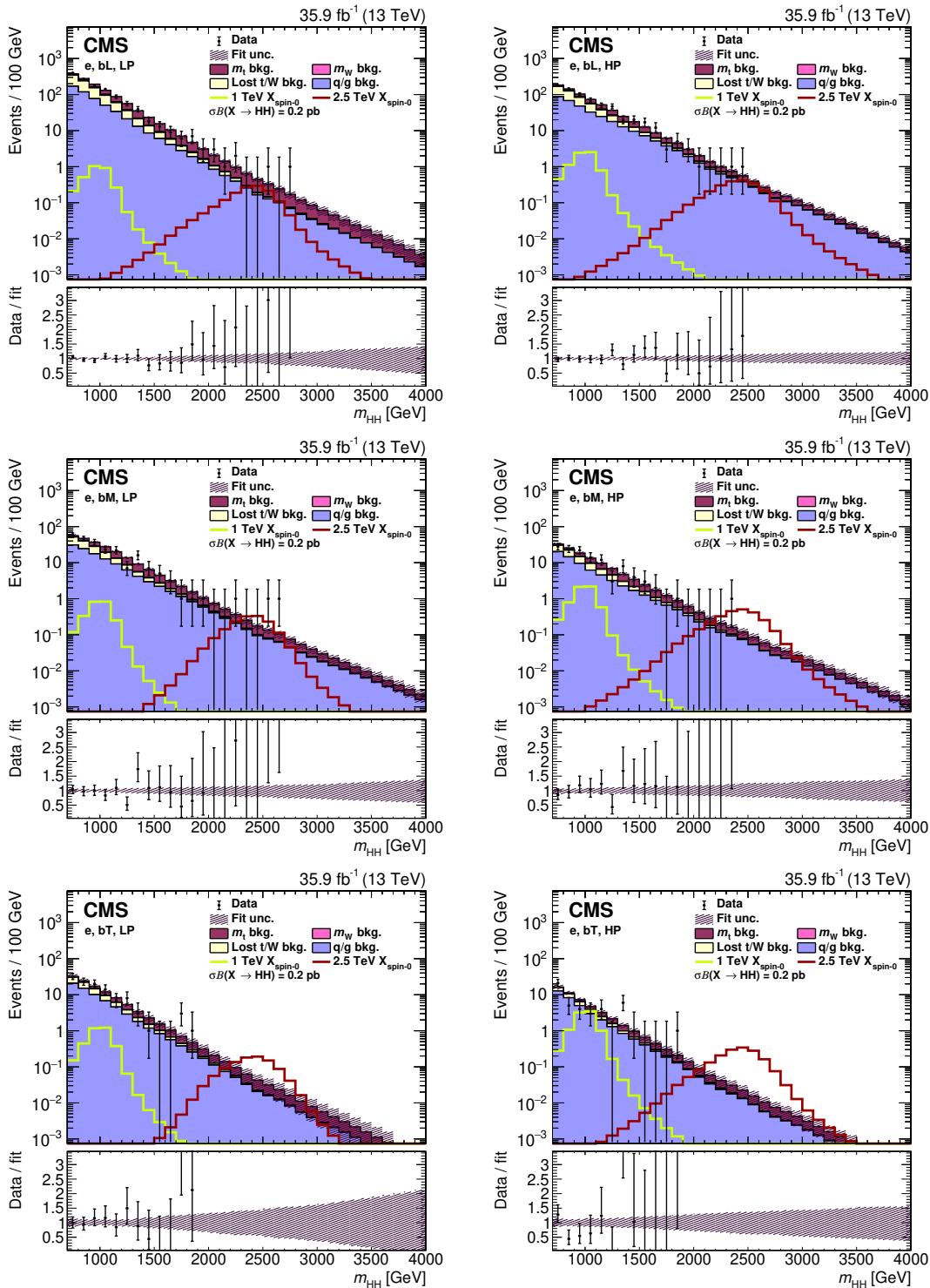
Figure 5. The fit result compared to data projected in m_{HH} for the electron event categories. The fit result is the filled histogram, with the different colors indicating different background categories. The background shape uncertainty is shown as the hatched band. Example spin-0 signal distributions for m_X of 1 and 2.5 TeV are shown as solid lines, with the product of the cross section and branching fraction to two Higgs bosons set to 0.2 pb. The lower panels show the ratio of the data to the fit result.
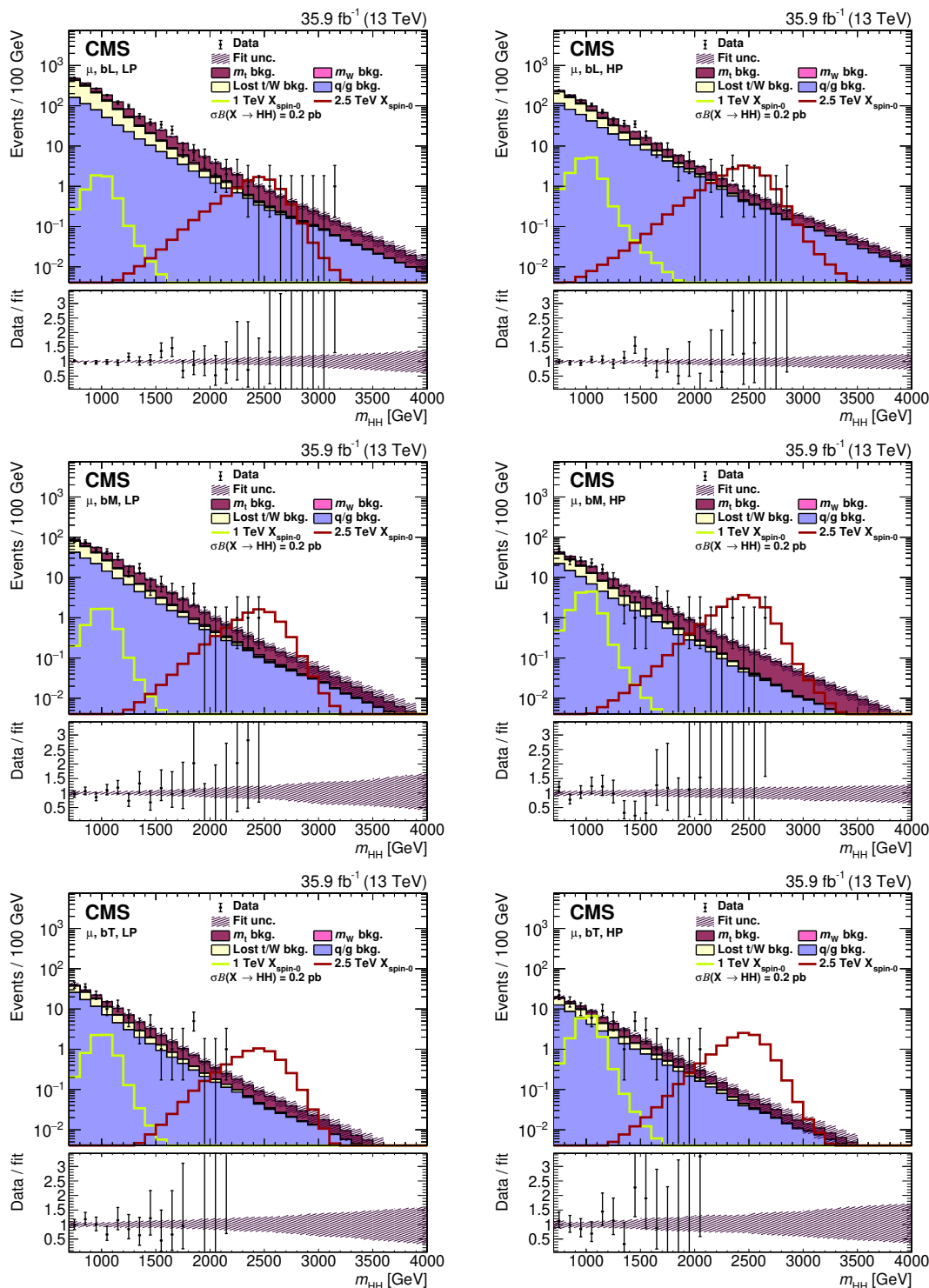
Figure 6. The fit result compared to data projected in m_{HH} for the muon event categories. The fit result is the filled histogram, with the different colors indicating different background categories. The background shape uncertainty is shown as the hatched band. Example spin-0 signal distributions for m_X of 1 and 2.5 TeV are shown as solid lines, with the product of the cross section and branching fraction to two Higgs bosons set to 0.2 pb. The lower panels show the ratio of the data to the fit result.
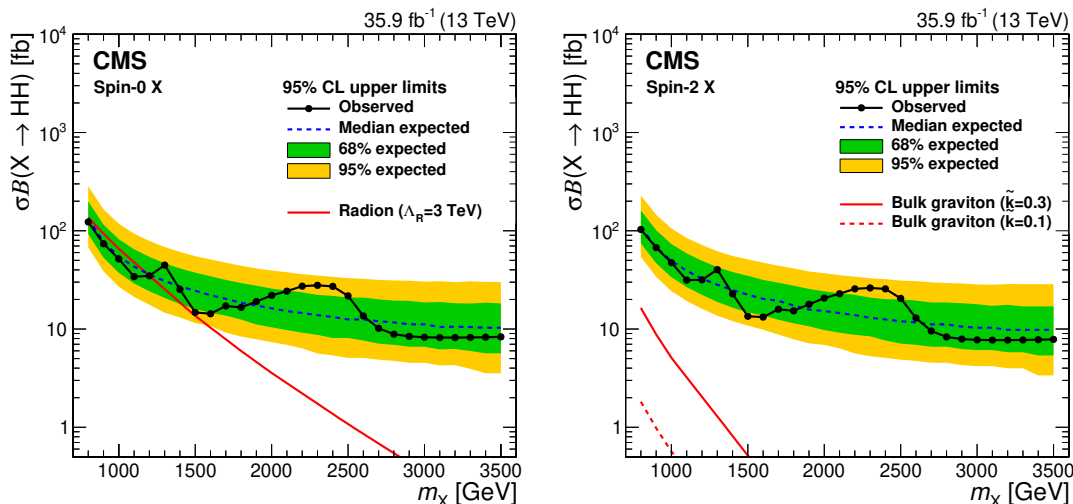
Figure 7. Observed and expected 95% CL upper limits on the product of the cross section and branching fraction to HH for a generic spin-0 (left) and spin-2 (right) boson X, as a function of mass. Example radion and bulk graviton predictions are also shown. The HH branching fraction is assumed to be 25 and 10%, respectively.

data are consistent with the expected standard model background. The results represent upper limits on the product of cross section and branching fraction for new bosons decaying to HH. The observed limit at 95% confidence level for a spin-0 resonance ranges from 123 fb at 0.8 TeV to 8.3 fb at 3.5 TeV, while the limit for a spin-2 resonance is 103 fb at 0.8 TeV and 7.8 fb at 3.5 TeV. These are the best results to date from searches for an HH resonance decaying to this final state. The results are comparable to the results from searches in other channels for resonances with masses below 1.5 TeV.

Acknowledgments

References

[1] ATLAS collaboration, *Observation of a new particle in the search for the Standard Model Higgs boson with the ATLAS detector at the LHC*, *Phys. Lett.* **B 716** (2012) 1 [arXiv:1207.7214] [INSPIRE].

[2] CMS collaboration, *Observation of a New Boson at a Mass of* 125 *GeV with the CMS Experiment at the LHC*, *Phys. Lett.* **B 716** (2012) 30 [arXiv:1207.7235] [INSPIRE].

[3] CMS collaboration, *Observation of a New Boson with Mass Near* 125 *GeV in pp Collisions at* $\sqrt{s} = 7$ *and* 8 *TeV*, *JHEP* **06** (2013) 081 [arXiv:1303.4571] [INSPIRE].

[4] F. Englert and R. Brout, *Broken Symmetry and the Mass of Gauge Vector Mesons*, *Phys. Rev. Lett.* **13** (1964) 321 [INSPIRE].

[5] P.W. Higgs, *Broken Symmetries and the Masses of Gauge Bosons*, *Phys. Rev. Lett.* **13** (1964) 508 [INSPIRE].

[6] G.C. Branco, P.M. Ferreira, L. Lavoura, M.N. Rebelo, M. Sher and J.P. Silva, *Theory and phenomenology of two-Higgs-doublet models*, *Phys. Rept.* **516** (2012) 1 [arXiv:1106.0034] [INSPIRE].

[7] P. Ramond, *Dual Theory for Free Fermions*, *Phys. Rev.* **D 3** (1971) 2415 [INSPIRE].

[8] Y.A. Golfand and E.P. Likhtman, *Extension of the Algebra of Poincaré Group Generators and Violation of p Invariance*, *JETP Lett.* **13** (1971) 323 [INSPIRE].

[9] A. Neveu and J.H. Schwarz, *Factorizable dual model of pions*, *Nucl. Phys.* **B 31** (1971) 86 [INSPIRE].

[10] D.V. Volkov and V.P. Akulov, *Possible universal neutrino interaction*, *JETP Lett.* **16** (1972) 438 [ɪɴSPIRE].

[11] J. Wess and B. Zumino, *A Lagrangian Model Invariant Under Supergauge Transformations*, *Phys. Lett.* **B 49** (1974) 52 [ɪɴSPIRE].

[12] J. Wess and B. Zumino, *Supergauge Transformations in Four-Dimensions*, *Nucl. Phys.* **B 70** (1974) 39 [ɪɴSPIRE].

[13] P. Fayet, *Supergauge Invariant Extension of the Higgs Mechanism and a Model for the electron and Its Neutrino*, *Nucl. Phys.* **B 90** (1975) 104 [ɪɴSPIRE].

[14] H.P. Nilles, *Supersymmetry, Supergravity and Particle Physics*, *Phys. Rept.* **110** (1984) 1 [ɪɴSPIRE].

[15] L. Randall and R. Sundrum, *A Large mass hierarchy from a small extra dimension*, *Phys. Rev. Lett.* **83** (1999) 3370 [hep-ph/9905221] [ɪɴSPIRE].

[16] W.D. Goldberger and M.B. Wise, *Modulus stabilization with bulk fields*, *Phys. Rev. Lett.* **83** (1999) 4922 [hep-ph/9907447] [ɪɴSPIRE].

[17] O. DeWolfe, D.Z. Freedman, S.S. Gubser and A. Karch, *Modeling the fifth-dimension with scalars and gravity*, *Phys. Rev.* **D 62** (2000) 046008 [hep-th/9909134] [ɪɴSPIRE].

[18] C. Csáki, M. Graesser, L. Randall and J. Terning, *Cosmology of brane models with radion stabilization*, *Phys. Rev.* **D 62** (2000) 045015 [hep-ph/9911406] [ɪɴSPIRE].

[19] C. Csáki, M.L. Graesser and G.D. Kribs, *Radion dynamics and electroweak physics*, *Phys. Rev.* **D 63** (2001) 065002 [hep-th/0008151] [ɪɴSPIRE].

[20] H. Davoudiasl, J.L. Hewett and T.G. Rizzo, *Phenomenology of the Randall-Sundrum Gauge Hierarchy Model*, *Phys. Rev. Lett.* **84** (2000) 2080 [hep-ph/9909255] [ɪɴSPIRE].

[21] K. Agashe, H. Davoudiasl, G. Perez and A. Soni, *Warped Gravitons at the LHC and Beyond*, *Phys. Rev.* **D 76** (2007) 036006 [hep-ph/0701186] [ɪɴSPIRE].

[22] A.L. Fitzpatrick, J. Kaplan, L. Randall and L.-T. Wang, *Searching for the Kaluza-Klein Graviton in Bulk RS Models*, *JHEP* **09** (2007) 013 [hep-ph/0701150] [ɪɴSPIRE].

[23] ATLAS collaboration, *Search for WZ resonances in the fully leptonic channel using pp collisions at $\sqrt{s} = 8\,TeV$ with the ATLAS detector*, *Phys. Lett.* **B 737** (2014) 223 [arXiv:1406.4456] [ɪɴSPIRE].

[24] ATLAS collaboration, *Search For Higgs Boson Pair Production in the $\gamma\gamma b\bar{b}$ Final State using pp Collision Data at $\sqrt{s} = 8\,TeV$ from the ATLAS Detector*, *Phys. Rev. Lett.* **114** (2015) 081802 [arXiv:1406.5053] [ɪɴSPIRE].

[25] ATLAS collaboration, *Searches for Higgs boson pair production in the $hh \to bb\tau\tau$, $\gamma\gamma WW^*$, $\gamma\gamma bb$, bbbb channels with the ATLAS detector*, *Phys. Rev.* **D 92** (2015) 092004 [arXiv:1509.04670] [ɪɴSPIRE].

[26] ATLAS collaboration, *Search for a new resonance decaying to a W or Z boson and a Higgs boson in the $\ell\ell/\ell\nu/\nu\nu + b\bar{b}$ final states with the ATLAS detector*, *Eur. Phys. J.* **C 75** (2015) 263 [arXiv:1503.08089] [ɪɴSPIRE].

[27] ATLAS collaboration, *Search for Higgs boson pair production in the $b\bar{b}b\bar{b}$ final state from pp collisions at $\sqrt{s} = 8\,TeV$ with the ATLAS detector*, *Eur. Phys. J.* **C 75** (2015) 412 [arXiv:1506.00285] [ɪɴSPIRE].

[28] ATLAS collaboration, *Search for heavy resonances decaying to a W or Z boson and a Higgs boson in the $q\bar{q}^{(\prime)}b\bar{b}$ final state in pp collisions at $\sqrt{s} = 13\,TeV$ with the ATLAS detector*, *Phys. Lett.* **B 774** (2017) 494 [arXiv:1707.06958] [INSPIRE].

[29] ATLAS collaboration, *Search for WW/WZ resonance production in $\ell\nu qq$ final states in pp collisions at $\sqrt{s} = 13\,TeV$ with the ATLAS detector*, *JHEP* **03** (2018) 042 [arXiv:1710.07235] [INSPIRE].

[30] ATLAS collaboration, *Search for heavy resonances decaying into WW in the $e\nu\mu\nu$ final state in pp collisions at $\sqrt{s} = 13\,TeV$ with the ATLAS detector*, *Eur. Phys. J.* **C 78** (2018) 24 [arXiv:1710.01123] [INSPIRE].

[31] ATLAS collaboration, *Searches for heavy ZZ and ZW resonances in the $\ell\ell qq$ and $\nu\nu qq$ final states in pp collisions at $\sqrt{s} = 13\,TeV$ with the ATLAS detector*, *JHEP* **03** (2018) 009 [arXiv:1708.09638] [INSPIRE].

[32] ATLAS collaboration, *Search for heavy ZZ resonances in the $\ell^+\ell^-\ell^+\ell^-$ and $\ell^+\ell^-\nu\bar{\nu}$ final states using proton-proton collisions at $\sqrt{s} = 13\,TeV$ with the ATLAS detector*, *Eur. Phys. J.* **C 78** (2018) 293 [arXiv:1712.06386] [INSPIRE].

[33] ATLAS collaboration, *Search for heavy resonances decaying into a W or Z boson and a Higgs boson in final states with leptons and b-jets in $36\,fb^{-1}$ of $\sqrt{s} = 13\,TeV$ pp collisions with the ATLAS detector*, *JHEP* **03** (2018) 174 [*Erratum JHEP* **11** (2018) 051] [arXiv:1712.06518] [INSPIRE].

[34] ATLAS collaboration, *Search for diboson resonances with boson-tagged jets in pp collisions at $\sqrt{s} = 13\,TeV$ with the ATLAS detector*, *Phys. Lett.* **B 777** (2018) 91 [arXiv:1708.04445] [INSPIRE].

[35] ATLAS collaboration, *Search for resonant WZ production in the fully leptonic final state in proton-proton collisions at $\sqrt{s} = 13\,TeV$ with the ATLAS detector*, *Phys. Lett.* **B 787** (2018) 68 [arXiv:1806.01532] [INSPIRE].

[36] ATLAS collaboration, *Search for resonant and non-resonant Higgs boson pair production in the $b\bar{b}\tau^+\tau^-$ decay channel in pp collisions at $\sqrt{s} = 13\,TeV$ with the ATLAS detector*, *Phys. Rev. Lett.* **121** (2018) 191801 [*Erratum ibid.* **122** (2019) 089901] [arXiv:1808.00336] [INSPIRE].

[37] ATLAS collaboration, *Search for pair production of Higgs bosons in the $b\bar{b}b\bar{b}$ final state using proton-proton collisions at $\sqrt{s} = 13\,TeV$ with the ATLAS detector*, *JHEP* **01** (2019) 030 [arXiv:1804.06174] [INSPIRE].

[38] ATLAS collaboration, *Search for Higgs boson pair production in the $b\bar{b}WW^*$ decay mode at $\sqrt{s} = 13\,TeV$ with the ATLAS detector*, *JHEP* **04** (2019) 092 [arXiv:1811.04671] [INSPIRE].

[39] CMS collaboration, *Search for new resonances decaying via WZ to leptons in proton-proton collisions at $\sqrt{s} = 8\,TeV$*, *Phys. Lett.* **B 740** (2015) 83 [arXiv:1407.3476] [INSPIRE].

[40] CMS collaboration, *Search for Narrow High-Mass Resonances in Proton-Proton Collisions at $\sqrt{s} = 8\,TeV$ Decaying to a Z and a Higgs Boson*, *Phys. Lett.* **B 748** (2015) 255 [arXiv:1502.04994] [INSPIRE].

[41] CMS collaboration, *Search for resonant pair production of Higgs bosons decaying to two bottom quark-antiquark pairs in proton-proton collisions at $8\,TeV$*, *Phys. Lett.* **B 749** (2015) 560 [arXiv:1503.04114] [INSPIRE].

[42] CMS collaboration, *Search for a massive resonance decaying into a Higgs boson and a W or Z boson in hadronic final states in proton-proton collisions at $\sqrt{s} = 8\,TeV$, JHEP* **02** (2016) 145 [arXiv:1506.01443] [INSPIRE].

[43] CMS collaboration, *Searches for a heavy scalar boson H decaying to a pair of 125 GeV Higgs bosons hh or for a heavy pseudoscalar boson A decaying to Zh, in the final states with $h \to \tau\tau$, Phys. Lett.* **B 755** (2016) 217 [arXiv:1510.01181] [INSPIRE].

[44] CMS collaboration, *Search for massive WH resonances decaying into the $\ell\nu b\bar{b}$ final state at $\sqrt{s} = 8\,TeV$, Eur. Phys. J.* **C 76** (2016) 237 [arXiv:1601.06431] [INSPIRE].

[45] CMS collaboration, *Search for heavy resonances decaying into a vector boson and a Higgs boson in final states with charged leptons, neutrinos and b quarks, Phys. Lett.* **B 768** (2017) 137 [arXiv:1610.08066] [INSPIRE].

[46] CMS collaboration, *Search for massive resonances decaying into WW, WZ or ZZ bosons in proton-proton collisions at $\sqrt{s} = 13\,TeV$, JHEP* **03** (2017) 162 [arXiv:1612.09159] [INSPIRE].

[47] CMS collaboration, *Search for heavy resonances that decay into a vector boson and a Higgs boson in hadronic final states at $\sqrt{s} = 13\,TeV$, Eur. Phys. J.* **C 77** (2017) 636 [arXiv:1707.01303] [INSPIRE].

[48] CMS collaboration, *Combination of searches for heavy resonances decaying to WW, WZ, ZZ, WH and ZH boson pairs in proton-proton collisions at $\sqrt{s} = 8$ and 13 TeV, Phys. Lett.* **B 774** (2017) 533 [arXiv:1705.09171] [INSPIRE].

[49] CMS collaboration, *Search for massive resonances decaying into WW, WZ, ZZ, qW and qZ with dijet final states at $\sqrt{s} = 13\,TeV$, Phys. Rev.* **D 97** (2018) 072006 [arXiv:1708.05379] [INSPIRE].

[50] CMS collaboration, *Search for a massive resonance decaying to a pair of Higgs bosons in the four b quark final state in proton-proton collisions at $\sqrt{s} = 13\,TeV$, Phys. Lett.* **B 781** (2018) 244 [arXiv:1710.04960] [INSPIRE].

[51] CMS collaboration, *Search for ZZ resonances in the $2\ell2\nu$ final state in proton-proton collisions at 13 TeV, JHEP* **03** (2018) 003 [arXiv:1711.04370] [INSPIRE].

[52] CMS collaboration, *Search for a heavy resonance decaying to a pair of vector bosons in the lepton plus merged jet final state at $\sqrt{s} = 13\,TeV$, JHEP* **05** (2018) 088 [arXiv:1802.09407] [INSPIRE].

[53] CMS collaboration, *Search for heavy resonances decaying into a vector boson and a Higgs boson in final states with charged leptons, neutrinos and b quarks at $\sqrt{s} = 13\,TeV$, JHEP* **11** (2018) 172 [arXiv:1807.02826] [INSPIRE].

[54] CMS collaboration, *Search for a heavy resonance decaying into a Z boson and a vector boson in the $\nu\bar{\nu}q\bar{q}$ final state, JHEP* **07** (2018) 075 [arXiv:1803.03838] [INSPIRE].

[55] CMS collaboration, *Search for a heavy resonance decaying into a Z boson and a Z or W boson in $2\ell2q$ final states at $\sqrt{s} = 13\,TeV$, JHEP* **09** (2018) 101 [arXiv:1803.10093] [INSPIRE].

[56] CMS collaboration, *Search for heavy resonances decaying into two Higgs bosons or into a Higgs boson and a W or Z boson in proton-proton collisions at 13 TeV, JHEP* **01** (2019) 051 [arXiv:1808.01365] [INSPIRE].

[57] CMS collaboration, *Search for production of Higgs boson pairs in the four b quark final state using large-area jets in proton-proton collisions at $\sqrt{s} = 13\,TeV$*, *JHEP* **01** (2019) 040 [arXiv:1808.01473] [INSPIRE].

[58] CMS collaboration, *The CMS trigger system*, 2017 *JINST* **12** P01020 [arXiv:1609.02366] [INSPIRE].

[59] CMS collaboration, *The CMS Experiment at the CERN LHC*, 2008 *JINST* **3** S08004 [INSPIRE].

[60] J. Alwall et al., *The automated computation of tree-level and next-to-leading order differential cross sections and their matching to parton shower simulations*, *JHEP* **07** (2014) 079 [arXiv:1405.0301] [INSPIRE].

[61] J. Alwall et al., *Comparative study of various algorithms for the merging of parton showers and matrix elements in hadronic collisions*, *Eur. Phys. J.* **C 53** (2008) 473 [arXiv:0706.2569] [INSPIRE].

[62] R. Frederix and S. Frixione, *Merging meets matching in MC@NLO*, *JHEP* **12** (2012) 061 [arXiv:1209.6215] [INSPIRE].

[63] P. Nason, *A New method for combining NLO QCD with shower Monte Carlo algorithms*, *JHEP* **11** (2004) 040 [hep-ph/0409146] [INSPIRE].

[64] S. Frixione, P. Nason and C. Oleari, *Matching NLO QCD computations with Parton Shower simulations: the POWHEG method*, *JHEP* **11** (2007) 070 [arXiv:0709.2092] [INSPIRE].

[65] S. Alioli, P. Nason, C. Oleari and E. Re, *A general framework for implementing NLO calculations in shower Monte Carlo programs: the POWHEG BOX*, *JHEP* **06** (2010) 043 [arXiv:1002.2581] [INSPIRE].

[66] E. Re, *Single-top Wt-channel production matched with parton showers using the POWHEG method*, *Eur. Phys. J.* **C 71** (2011) 1547 [arXiv:1009.2450] [INSPIRE].

[67] T. Melia, P. Nason, R. Röntsch and G. Zanderighi, *W^+W^-, WZ and ZZ production in the POWHEG BOX*, *JHEP* **11** (2011) 078 [arXiv:1107.5051] [INSPIRE].

[68] P. Nason and G. Zanderighi, *W^+W^-, WZ and ZZ production in the POWHEG-BOX-V2*, *Eur. Phys. J.* **C 74** (2014) 2702 [arXiv:1311.1365] [INSPIRE].

[69] R. Frederix, E. Re and P. Torrielli, *Single-top t-channel hadroproduction in the four-flavour scheme with POWHEG and aMC@NLO*, *JHEP* **09** (2012) 130 [arXiv:1207.5391] [INSPIRE].

[70] H.B. Hartanto, B. Jager, L. Reina and D. Wackeroth, *Higgs boson production in association with top quarks in the POWHEG BOX*, *Phys. Rev.* **D 91** (2015) 094003 [arXiv:1501.04498] [INSPIRE].

[71] T. Sjöstrand et al., *An Introduction to PYTHIA 8.2*, *Comput. Phys. Commun.* **191** (2015) 159 [arXiv:1410.3012] [INSPIRE].

[72] CMS collaboration, *Event generator tunes obtained from underlying event and multiparton scattering measurements*, *Eur. Phys. J.* **C 76** (2016) 155 [arXiv:1512.00815] [INSPIRE].

[73] R.D. Ball et al., *Impact of Heavy Quark Masses on Parton Distributions and LHC Phenomenology*, *Nucl. Phys.* **B 849** (2011) 296 [arXiv:1101.1300] [INSPIRE].

[74] GEANT4 collaboration, *GEANT4: A Simulation toolkit*, *Nucl. Instrum. Meth.* **A 506** (2003) 250 [INSPIRE].

[75] M. Czakon and A. Mitov, *Top++: A Program for the Calculation of the Top-Pair Cross-Section at Hadron Colliders*, *Comput. Phys. Commun.* **185** (2014) 2930 [arXiv:1112.5675] [INSPIRE].

[76] Y. Li and F. Petriello, *Combining QCD and electroweak corrections to dilepton production in FEWZ*, *Phys. Rev.* **D 86** (2012) 094034 [arXiv:1208.5967] [INSPIRE].

[77] J.M. Campbell, R.K. Ellis and C. Williams, *Vector boson pair production at the LHC*, *JHEP* **07** (2011) 018 [arXiv:1105.0020] [INSPIRE].

[78] J.M. Campbell and R.K. Ellis, *Top-Quark Processes at NLO in Production and Decay*, *J. Phys.* **G 42** (2015) 015005 [arXiv:1204.1513] [INSPIRE].

[79] J.M. Campbell, R.K. Ellis and F. Tramontano, *Single top production and decay at next-to-leading order*, *Phys. Rev.* **D 70** (2004) 094012 [hep-ph/0408158] [INSPIRE].

[80] LHC HIGGS CROSS SECTION WORKING GROUP collaboration, *Handbook of LHC Higgs Cross Sections: 4. Deciphering the Nature of the Higgs Sector*, arXiv:1610.07922 [INSPIRE].

[81] CMS collaboration, *Particle-flow reconstruction and global event description with the CMS detector*, 2017 *JINST* **12** P10003 [arXiv:1706.04965] [INSPIRE].

[82] M. Cacciari, G.P. Salam and G. Soyez, *The anti-k_t jet clustering algorithm*, *JHEP* **04** (2008) 063 [arXiv:0802.1189] [INSPIRE].

[83] M. Cacciari, G.P. Salam and G. Soyez, *FastJet User Manual*, *Eur. Phys. J.* **C 72** (2012) 1896 [arXiv:1111.6097] [INSPIRE].

[84] CMS collaboration, *Performance of Electron Reconstruction and Selection with the CMS Detector in Proton-Proton Collisions at $\sqrt{s} = 8$ TeV*, 2015 *JINST* **10** P06005 [arXiv:1502.02701] [INSPIRE].

[85] CMS collaboration, *Performance of the CMS muon detector and muon reconstruction with proton-proton collisions at $\sqrt{s} = 13$ TeV*, 2018 *JINST* **13** P06015 [arXiv:1804.04528] [INSPIRE].

[86] K. Rehermann and B. Tweedie, *Efficient Identification of Boosted Semileptonic Top Quarks at the LHC*, *JHEP* **03** (2011) 059 [arXiv:1007.2221] [INSPIRE].

[87] CMS collaboration, *Measurements of Inclusive W and Z Cross Sections in pp Collisions at $\sqrt{s} = 7$ TeV*, *JHEP* **01** (2011) 080 [arXiv:1012.2466] [INSPIRE].

[88] D. Bertolini, P. Harris, M. Low and N. Tran, *Pileup Per Particle Identification*, *JHEP* **10** (2014) 059 [arXiv:1407.6013] [INSPIRE].

[89] CMS collaboration, *Jet algorithms performance in 13 TeV data*, CMS-PAS-JME-16-003 (2017) [INSPIRE].

[90] CMS collaboration, *Jet energy scale and resolution in the CMS experiment in pp collisions at 8 TeV*, 2017 *JINST* **12** P02014 [arXiv:1607.03663] [INSPIRE].

[91] Y.L. Dokshitzer, G.D. Leder, S. Moretti and B.R. Webber, *Better jet clustering algorithms*, *JHEP* **08** (1997) 001 [hep-ph/9707323] [INSPIRE].

[92] M. Wobisch and T. Wengler, *Hadronization corrections to jet cross-sections in deep inelastic scattering*, in proceedings of the *Workshop on Monte Carlo Generators for HERA Physics (Plenary Starting Meeting)*, Hamburg, Germany, 27–30 April 1998, pp. 270–279 [hep-ph/9907280] [INSPIRE].

[93] M. Dasgupta, A. Fregoso, S. Marzani and G.P. Salam, *Towards an understanding of jet substructure*, *JHEP* **09** (2013) 029 [arXiv:1307.0007] [INSPIRE].

[94] J.M. Butterworth, A.R. Davison, M. Rubin and G.P. Salam, *Jet substructure as a new Higgs search channel at the LHC*, *Phys. Rev. Lett.* **100** (2008) 242001 [arXiv:0802.2470] [INSPIRE].

[95] A.J. Larkoski, S. Marzani, G. Soyez and J. Thaler, *Soft Drop*, *JHEP* **05** (2014) 146 [arXiv:1402.2657] [INSPIRE].

[96] J. Thaler and K. Van Tilburg, *Identifying Boosted Objects with N-subjettiness*, *JHEP* **03** (2011) 015 [arXiv:1011.2268] [INSPIRE].

[97] S. Catani, Y.L. Dokshitzer, M.H. Seymour and B.R. Webber, *Longitudinally invariant K_t clustering algorithms for hadron hadron collisions*, *Nucl. Phys.* **B 406** (1993) 187 [INSPIRE].

[98] ATLAS and CMS collaborations, *Combined Measurement of the Higgs Boson Mass in pp Collisions at $\sqrt{s} = 7$ and 8 TeV with the ATLAS and CMS Experiments*, *Phys. Rev. Lett.* **114** (2015) 191803 [arXiv:1503.07589] [INSPIRE].

[99] CMS collaboration, *Identification of heavy-flavour jets with the CMS detector in pp collisions at 13 TeV*, 2018 *JINST* **13** P05011 [arXiv:1712.07158] [INSPIRE].

[100] CMS collaboration, *Performance of missing transverse momentum in pp collisions at $\sqrt{s} = 13$ TeV using the CMS detector*, CMS-PAS-JME-17-001 (2018) [INSPIRE].

[101] CMS collaboration, *Measurement of normalized differential $t\bar{t}$ cross sections in the dilepton channel from pp collisions at $\sqrt{s} = 13$ TeV*, *JHEP* **04** (2018) 060 [arXiv:1708.07638] [INSPIRE].

[102] CMS collaboration, *Measurement of differential cross sections for top quark pair production using the lepton+jets final state in proton-proton collisions at 13 TeV*, *Phys. Rev.* **D 95** (2017) 092001 [arXiv:1610.04191] [INSPIRE].

[103] M. Rosenblatt, *Remarks on some nonparametric estimates of a density function*, *Ann. Math. Statist.* **27** (1956) 832.

[104] B.W. Silverman, *Density estimation for statistics and data analysis*, Chapman and Hall (1986).

[105] K.S. Cranmer, *Kernel estimation in high-energy physics*, *Comput. Phys. Commun.* **136** (2001) 198 [hep-ex/0011057] [INSPIRE].

[106] D.W. Scott, *Multivariate density estimation: theory, practice, and visualization*, John Wiley and Sons (1992).

[107] M.J. Oreglia, *A study of the reactions $\psi' \to \gamma\gamma\psi$*, Ph.D. Thesis, Stanford University, Stanford California U.S.A. (1980).

[108] J. Gaiser, *Charmonium spectroscopy from radiative decays of the J/ψ and ψ'*, Ph.D. Thesis, Stanford University, Stanford California U.S.A. (1982).

[109] CMS collaboration, *CMS Luminosity Measurements for the 2016 Data Taking Period*, CMS-PAS-LUM-17-001 (2017) [INSPIRE].

[110] M. Cacciari, S. Frixione, M.L. Mangano, P. Nason and G. Ridolfi, *The $t\bar{t}$ cross-section at 1.8 TeV and 1.96 TeV: A Study of the systematics due to parton densities and scale dependence*, *JHEP* **04** (2004) 068 [hep-ph/0303085] [INSPIRE].

[111] S. Catani, D. de Florian, M. Grazzini and P. Nason, *Soft gluon resummation for Higgs boson production at hadron colliders*, *JHEP* **07** (2003) 028 [hep-ph/0306211] [ɪɴSPIRE].

[112] S. Baker and R.D. Cousins, *Clarification of the use of CHI-square and likelihood functions in fits to histograms*, *Nucl. Instrum. Meth.* **221** (1984) 437 [ɪɴSPIRE].

[113] G. Cowan, K. Cranmer, E. Gross and O. Vitells, *Asymptotic formulae for likelihood-based tests of new physics*, *Eur. Phys. J.* **C 71** (2011) 1554 [*Erratum ibid.* **C 73** (2013) 2501] [arXiv:1007.1727] [ɪɴSPIRE].

[114] T. Junk, *Confidence level computation for combining searches with small statistics*, *Nucl. Instrum. Meth.* **A 434** (1999) 435 [hep-ex/9902006] [ɪɴSPIRE].

[115] A.L. Read, *Presentation of search results: The CL_s technique*, *J. Phys.* **G 28** (2002) 2693 [ɪɴSPIRE].

[116] A. Oliveira, *Gravity particles from Warped Extra Dimensions, predictions for LHC*, arXiv:1404.0102 [ɪɴSPIRE].

[117] M. Gouzevitch, A. Oliveira, J. Rojo, R. Rosenfeld, G.P. Salam and V. Sanz, *Scale-invariant resonance tagging in multijet events and new physics in Higgs pair production*, *JHEP* **07** (2013) 148 [arXiv:1303.6636] [ɪɴSPIRE].

The CMS collaboration

Yerevan Physics Institute, Yerevan, Armenia

A.M. Sirunyan[†], A. Tumasyan

Institut für Hochenergiephysik, Wien, Austria

W. Adam, F. Ambrogi, T. Bergauer, J. Brandstetter, M. Dragicevic, J. Erö, A. Escalante Del Valle, M. Flechl, R. Frühwirth[1], M. Jeitler[1], N. Krammer, I. Krätschmer, D. Liko, T. Madlener, I. Mikulec, N. Rad, J. Schieck[1], R. Schöfbeck, M. Spanring, D. Spitzbart, W. Waltenberger, J. Wittmann, C.-E. Wulz[1], M. Zarucki

Institute for Nuclear Problems, Minsk, Belarus

V. Drugakov, V. Mossolov, J. Suarez Gonzalez

Universiteit Antwerpen, Antwerpen, Belgium

M.R. Darwish, E.A. De Wolf, D. Di Croce, X. Janssen, J. Lauwers, A. Lelek, M. Pieters, H. Rejeb Sfar, H. Van Haevermaet, P. Van Mechelen, S. Van Putte, N. Van Remortel

Vrije Universiteit Brussel, Brussel, Belgium

F. Blekman, E.S. Bols, S.S. Chhibra, J. D'Hondt, J. De Clercq, D. Lontkovskyi, S. Lowette, I. Marchesini, S. Moortgat, L. Moreels, Q. Python, K. Skovpen, S. Tavernier, W. Van Doninck, P. Van Mulders, I. Van Parijs

Université Libre de Bruxelles, Bruxelles, Belgium

D. Beghin, B. Bilin, H. Brun, B. Clerbaux, G. De Lentdecker, H. Delannoy, B. Dorney, L. Favart, A. Grebenyuk, A.K. Kalsi, J. Luetic, A. Popov, N. Postiau, E. Starling, L. Thomas, C. Vander Velde, P. Vanlaer, D. Vannerom, Q. Wang

Ghent University, Ghent, Belgium

T. Cornelis, D. Dobur, I. Khvastunov[2], C. Roskas, D. Trocino, M. Tytgat, W. Verbeke, B. Vermassen, M. Vit, N. Zaganidis

Université Catholique de Louvain, Louvain-la-Neuve, Belgium

O. Bondu, G. Bruno, C. Caputo, P. David, C. Delaere, M. Delcourt, A. Giammanco, G. Krintiras, V. Lemaitre, A. Magitteri, K. Piotrzkowski, J. Prisciandaro, A. Saggio, M. Vidal Marono, P. Vischia, J. Zobec

Centro Brasileiro de Pesquisas Fisicas, Rio de Janeiro, Brazil

F.L. Alves, G.A. Alves, G. Correia Silva, C. Hensel, A. Moraes, P. Rebello Teles

Universidade do Estado do Rio de Janeiro, Rio de Janeiro, Brazil

E. Belchior Batista Das Chagas, W. Carvalho, J. Chinellato[3], E. Coelho, E.M. Da Costa, G.G. Da Silveira[4], D. De Jesus Damiao, C. De Oliveira Martins, S. Fonseca De Souza, L.M. Huertas Guativa, H. Malbouisson, J. Martins[5], D. Matos Figueiredo, M. Medina Jaime[6], M. Melo De Almeida, C. Mora Herrera, L. Mundim, H. Nogima, W.L. Prado Da Silva, L.J. Sanchez Rosas, A. Santoro, A. Sznajder, M. Thiel, E.J. Tonelli Manganote[3], F. Torres Da Silva De Araujo, A. Vilela Pereira

Universidade Estadual Paulista [a], Universidade Federal do ABC [b], São Paulo, Brazil

S. Ahuja[a], C.A. Bernardes[a], L. Calligaris[a], T.R. Fernandez Perez Tomei[a], E.M. Gregores[b], D.S. Lemos, P.G. Mercadante[b], S.F. Novaes[a], SandraS. Padula[a]

Institute for Nuclear Research and Nuclear Energy, Bulgarian Academy of Sciences, Sofia, Bulgaria

A. Aleksandrov, G. Antchev, R. Hadjiiska, P. Iaydjiev, A. Marinov, M. Misheva, M. Rodozov, M. Shopova, G. Sultanov

University of Sofia, Sofia, Bulgaria

A. Dimitrov, L. Litov, B. Pavlov, P. Petkov

Beihang University, Beijing, China

W. Fang[7], X. Gao[7], L. Yuan

Institute of High Energy Physics, Beijing, China

M. Ahmad, G.M. Chen, H.S. Chen, M. Chen, C.H. Jiang, D. Leggat, H. Liao, Z. Liu, S.M. Shaheen[8], A. Spiezia, J. Tao, E. Yazgan, H. Zhang, S. Zhang[8], J. Zhao

State Key Laboratory of Nuclear Physics and Technology, Peking University, Beijing, China

A. Agapitos, Y. Ban, G. Chen, A. Levin, J. Li, L. Li, Q. Li, Y. Mao, S.J. Qian, D. Wang

Tsinghua University, Beijing, China

Z. Hu, Y. Wang

Universidad de Los Andes, Bogota, Colombia

C. Avila, A. Cabrera, L.F. Chaparro Sierra, C. Florez, C.F. González Hernández, M.A. Segura Delgado

University of Split, Faculty of Electrical Engineering, Mechanical Engineering and Naval Architecture, Split, Croatia

D. Giljanović, N. Godinovic, D. Lelas, I. Puljak, T. Sculac

University of Split, Faculty of Science, Split, Croatia

Z. Antunovic, M. Kovac

Institute Rudjer Boskovic, Zagreb, Croatia

V. Brigljevic, S. Ceci, D. Ferencek, K. Kadija, B. Mesic, M. Roguljic, A. Starodumov[9], T. Susa

University of Cyprus, Nicosia, Cyprus

M.W. Ather, A. Attikis, E. Erodotou, A. Ioannou, M. Kolosova, S. Konstantinou, G. Mavromanolakis, J. Mousa, C. Nicolaou, F. Ptochos, P.A. Razis, H. Rykaczewski, D. Tsiakkouri

Charles University, Prague, Czech Republic

M. Finger[10], M. Finger Jr.[10], A. Kveton, J. Tomsa

Escuela Politecnica Nacional, Quito, Ecuador

E. Ayala

Universidad San Francisco de Quito, Quito, Ecuador

E. Carrera Jarrin

Academy of Scientific Research and Technology of the Arab Republic of Egypt, Egyptian Network of High Energy Physics, Cairo, Egypt

A. Ellithi Kamel[11], E. Salama[12,13]

National Institute of Chemical Physics and Biophysics, Tallinn, Estonia

S. Bhowmik, A. Carvalho Antunes De Oliveira, R.K. Dewanjee, K. Ehataht, M. Kadastik, M. Raidal, C. Veelken

Department of Physics, University of Helsinki, Helsinki, Finland

P. Eerola, L. Forthomme, H. Kirschenmann, K. Osterberg, J. Pekkanen, M. Voutilainen

Helsinki Institute of Physics, Helsinki, Finland

F. Garcia, J. Havukainen, J.K. Heikkilä, T. Järvinen, V. Karimäki, R. Kinnunen, T. Lampén, K. Lassila-Perini, S. Laurila, S. Lehti, T. Lindén, P. Luukka, T. Mäenpää, H. Siikonen, E. Tuominen, J. Tuominiemi

Lappeenranta University of Technology, Lappeenranta, Finland

T. Tuuva

IRFU, CEA, Université Paris-Saclay, Gif-sur-Yvette, France

M. Besancon, F. Couderc, M. Dejardin, D. Denegri, B. Fabbro, J.L. Faure, F. Ferri, S. Ganjour, A. Givernaud, P. Gras, G. Hamel de Monchenault, P. Jarry, C. Leloup, E. Locci, J. Malcles, J. Rander, A. Rosowsky, M.Ö. Sahin, A. Savoy-Navarro[14], M. Titov

Laboratoire Leprince-Ringuet, Ecole polytechnique, CNRS/IN2P3, Université Paris-Saclay, Palaiseau, France

C. Amendola, F. Beaudette, P. Busson, C. Charlot, B. Diab, R. Granier de Cassagnac, I. Kucher, A. Lobanov, C. Martin Perez, M. Nguyen, C. Ochando, P. Paganini, J. Rembser, R. Salerno, J.B. Sauvan, Y. Sirois, A. Zabi, A. Zghiche

Université de Strasbourg, CNRS, IPHC UMR 7178, Strasbourg, France

J.-L. Agram[15], J. Andrea, D. Bloch, G. Bourgatte, J.-M. Brom, E.C. Chabert, C. Collard, E. Conte[15], J.-C. Fontaine[15], D. Gelé, U. Goerlach, M. Jansová, A.-C. Le Bihan, N. Tonon, P. Van Hove

Centre de Calcul de l'Institut National de Physique Nucleaire et de Physique des Particules, CNRS/IN2P3, Villeurbanne, France

S. Gadrat

Université de Lyon, Université Claude Bernard Lyon 1, CNRS-IN2P3, Institut de Physique Nucléaire de Lyon, Villeurbanne, France

S. Beauceron, C. Bernet, G. Boudoul, C. Camen, N. Chanon, R. Chierici, D. Contardo, P. Depasse, H. El Mamouni, J. Fay, S. Gascon, M. Gouzevitch, B. Ille, Sa. Jain, F. Lagarde,

I.B. Laktineh, H. Lattaud, M. Lethuillier, L. Mirabito, S. Perries, V. Sordini, G. Touquet, M. Vander Donckt, S. Viret

Georgian Technical University, Tbilisi, Georgia
T. Toriashvili[16]

Tbilisi State University, Tbilisi, Georgia
Z. Tsamalaidze[10]

RWTH Aachen University, I. Physikalisches Institut, Aachen, Germany
C. Autermann, L. Feld, M.K. Kiesel, K. Klein, M. Lipinski, D. Meuser, A. Pauls, M. Preuten, M.P. Rauch, C. Schomakers, J. Schulz, M. Teroerde, B. Wittmer

RWTH Aachen University, III. Physikalisches Institut A, Aachen, Germany
A. Albert, M. Erdmann, S. Erdweg, T. Esch, B. Fischer, R. Fischer, S. Ghosh, T. Hebbeker, K. Hoepfner, H. Keller, L. Mastrolorenzo, M. Merschmeyer, A. Meyer, P. Millet, G. Mocellin, S. Mondal, S. Mukherjee, D. Noll, A. Novak, T. Pook, A. Pozdnyakov, T. Quast, M. Radziej, Y. Rath, H. Reithler, M. Rieger, A. Schmidt, S.C. Schuler, A. Sharma, S. Thüer, S. Wiedenbeck

RWTH Aachen University, III. Physikalisches Institut B, Aachen, Germany
G. Flügge, W. Haj Ahmad[17], O. Hlushchenko, T. Kress, T. Müller, A. Nehrkorn, A. Nowack, C. Pistone, O. Pooth, D. Roy, H. Sert, A. Stahl[18]

Deutsches Elektronen-Synchrotron, Hamburg, Germany
M. Aldaya Martin, C. Asawatangtrakuldee, P. Asmuss, I. Babounikau, H. Bakhshiansohi, K. Beernaert, O. Behnke, U. Behrens, A. Bermúdez Martínez, D. Bertsche, A.A. Bin Anuar, K. Borras[19], V. Botta, A. Campbell, A. Cardini, P. Connor, S. Consuegra Rodríguez, C. Contreras-Campana, V. Danilov, A. De Wit, M.M. Defranchis, C. Diez Pardos, D. Domínguez Damiani, G. Eckerlin, D. Eckstein, T. Eichhorn, A. Elwood, E. Eren, E. Gallo[20], A. Geiser, J.M. Grados Luyando, A. Grohsjean, M. Guthoff, M. Haranko, A. Harb, N.Z. Jomhari, H. Jung, A. Kasem[19], M. Kasemann, J. Keaveney, C. Kleinwort, J. Knolle, D. Krücker, W. Lange, T. Lenz, J. Leonard, J. Lidrych, K. Lipka, W. Lohmann[21], R. Mankel, I.-A. Melzer-Pellmann, A.B. Meyer, M. Meyer, M. Missiroli, G. Mittag, J. Mnich, A. Mussgiller, V. Myronenko, D. Pérez Adán, S.K. Pflitsch, D. Pitzl, A. Raspereza, A. Saibel, M. Savitskyi, V. Scheurer, P. Schütze, C. Schwanenberger, R. Shevchenko, A. Singh, H. Tholen, O. Turkot, A. Vagnerini, M. Van De Klundert, G.P. Van Onsem, R. Walsh, Y. Wen, K. Wichmann, C. Wissing, O. Zenaiev, R. Zlebcik

University of Hamburg, Hamburg, Germany
R. Aggleton, S. Bein, L. Benato, A. Benecke, V. Blobel, T. Dreyer, A. Ebrahimi, A. Fröhlich, C. Garbers, E. Garutti, D. Gonzalez, P. Gunnellini, J. Haller, A. Hinzmann, A. Karavdina, G. Kasieczka, R. Klanner, R. Kogler, N. Kovalchuk, S. Kurz, V. Kutzner, J. Lange, T. Lange, A. Malara, D. Marconi, J. Multhaup, M. Niedziela, C.E.N. Niemeyer, D. Nowatschin, A. Perieanu, A. Reimers, O. Rieger, C. Scharf, P. Schleper, S. Schumann, J. Schwandt, J. Sonneveld, H. Stadie, G. Steinbrück, F.M. Stober, M. Stöver, B. Vormwald, I. Zoi

Karlsruher Institut fuer Technologie, Karlsruhe, Germany

M. Akbiyik, C. Barth, M. Baselga, S. Baur, T. Berger, E. Butz, R. Caspart, T. Chwalek, W. De Boer, A. Dierlamm, K. El Morabit, N. Faltermann, M. Giffels, P. Goldenzweig, A. Gottmann, M.A. Harrendorf, F. Hartmann[18], U. Husemann, S. Kudella, S. Mitra, M.U. Mozer, Th. Müller, M. Musich, A. Nürnberg, G. Quast, K. Rabbertz, M. Schröder, I. Shvetsov, H.J. Simonis, R. Ulrich, M. Weber, C. Wöhrmann, R. Wolf

Institute of Nuclear and Particle Physics (INPP), NCSR Demokritos, Aghia Paraskevi, Greece

G. Anagnostou, P. Asenov, G. Daskalakis, T. Geralis, A. Kyriakis, D. Loukas, G. Paspalaki

National and Kapodistrian University of Athens, Athens, Greece

M. Diamantopoulou, G. Karathanasis, P. Kontaxakis, A. Panagiotou, I. Papavergou, N. Saoulidou, A. Stakia, K. Theofilatos, K. Vellidis

National Technical University of Athens, Athens, Greece

G. Bakas, K. Kousouris, I. Papakrivopoulos, G. Tsipolitis

University of Ioánnina, Ioánnina, Greece

I. Evangelou, C. Foudas, P. Gianneios, P. Katsoulis, P. Kokkas, S. Mallios, K. Manitara, N. Manthos, I. Papadopoulos, J. Strologas, F.A. Triantis, D. Tsitsonis

MTA-ELTE Lendület CMS Particle and Nuclear Physics Group, Eötvös Loránd University, Budapest, Hungary

M. Bartók[22], M. Csanad, P. Major, K. Mandal, A. Mehta, M.I. Nagy, G. Pasztor, O. Surányi, G.I. Veres

Wigner Research Centre for Physics, Budapest, Hungary

G. Bencze, C. Hajdu, D. Horvath[23], F. Sikler, T.Á. Vámi, V. Veszpremi, G. Vesztergombi[†]

Institute of Nuclear Research ATOMKI, Debrecen, Hungary

N. Beni, S. Czellar, J. Karancsi[22], A. Makovec, J. Molnar, Z. Szillasi

Institute of Physics, University of Debrecen, Debrecen, Hungary

P. Raics, D. Teyssier, Z.L. Trocsanyi, B. Ujvari

Eszterhazy Karoly University, Karoly Robert Campus, Gyongyos, Hungary

T.F. Csorgo, W.J. Metzger, F. Nemes, T. Novak

Indian Institute of Science (IISc), Bangalore, India

S. Choudhury, J.R. Komaragiri, P.C. Tiwari

National Institute of Science Education and Research, HBNI, Bhubaneswar, India

S. Bahinipati[25], C. Kar, G. Kole, P. Mal, V.K. Muraleedharan Nair Bindhu, A. Nayak[26], S. Roy Chowdhury, D.K. Sahoo[25], S.K. Swain

Panjab University, Chandigarh, India

S. Bansal, S.B. Beri, V. Bhatnagar, S. Chauhan, R. Chawla, N. Dhingra, R. Gupta, A. Kaur, M. Kaur, S. Kaur, P. Kumari, M. Lohan, M. Meena, K. Sandeep, S. Sharma, J.B. Singh, A.K. Virdi, G. Walia

University of Delhi, Delhi, India

A. Bhardwaj, B.C. Choudhary, R.B. Garg, M. Gola, S. Keshri, Ashok Kumar, S. Malhotra, M. Naimuddin, P. Priyanka, K. Ranjan, Aashaq Shah, R. Sharma

Saha Institute of Nuclear Physics, HBNI, Kolkata, India

R. Bhardwaj[27], M. Bharti[27], R. Bhattacharya, S. Bhattacharya, U. Bhawandeep[27], D. Bhowmik, S. Dey, S. Dutta, S. Ghosh, M. Maity[28], K. Mondal, S. Nandan, A. Purohit, P.K. Rout, A. Roy, G. Saha, S. Sarkar, T. Sarkar[28], M. Sharan, B. Singh[27], S. Thakur[27]

Indian Institute of Technology Madras, Madras, India

P.K. Behera, P. Kalbhor, A. Muhammad, P.R. Pujahari, A. Sharma, A.K. Sikdar

Bhabha Atomic Research Centre, Mumbai, India

R. Chudasama, D. Dutta, V. Jha, V. Kumar, D.K. Mishra, P.K. Netrakanti, L.M. Pant, P. Shukla

Tata Institute of Fundamental Research-A, Mumbai, India

T. Aziz, M.A. Bhat, S. Dugad, G.B. Mohanty, N. Sur, RavindraKumar Verma

Tata Institute of Fundamental Research-B, Mumbai, India

S. Banerjee, S. Bhattacharya, S. Chatterjee, P. Das, M. Guchait, S. Karmakar, S. Kumar, G. Majumder, K. Mazumdar, S. Sawant

Indian Institute of Science Education and Research (IISER), Pune, India

S. Chauhan, S. Dube, V. Hegde, A. Kapoor, K. Kothekar, S. Pandey, A. Rane, A. Rastogi, S. Sharma

Institute for Research in Fundamental Sciences (IPM), Tehran, Iran

S. Chenarani[29], E. Eskandari Tadavani, S.M. Etesami[29], M. Khakzad, M. Mohammadi Najafabadi, M. Naseri, F. Rezaei Hosseinabadi

University College Dublin, Dublin, Ireland

M. Felcini, M. Grunewald

INFN Sezione di Bari [a], Università di Bari [b], Politecnico di Bari [c], Bari, Italy

M. Abbrescia[a,b], C. Calabria[a,b], A. Colaleo[a], D. Creanza[a,c], L. Cristella[a,b], N. De Filippis[a,c], M. De Palma[a,b], A. Di Florio[a,b], L. Fiore[a], A. Gelmi[a,b], G. Iaselli[a,c], M. Ince[a,b], S. Lezki[a,b], G. Maggi[a,c], M. Maggi[a], G. Miniello[a,b], S. My[a,b], S. Nuzzo[a,b], A. Pompili[a,b], G. Pugliese[a,c], R. Radogna[a], A. Ranieri[a], G. Selvaggi[a,b], L. Silvestris[a], R. Venditti[a], P. Verwilligen[a]

INFN Sezione di Bologna [a], Università di Bologna [b], Bologna, Italy

G. Abbiendi[a], C. Battilana[a,b], D. Bonacorsi[a,b], L. Borgonovi[a,b], S. Braibant-Giacomelli[a,b], R. Campanini[a,b], P. Capiluppi[a,b], A. Castro[a,b], F.R. Cavallo[a], C. Ciocca[a], G. Codispoti[a,b],

M. Cuffiani[a,b], G.M. Dallavalle[a], F. Fabbri[a], A. Fanfani[a,b], E. Fontanesi, P. Giacomelli[a], C. Grandi[a], L. Guiducci[a,b], F. Iemmi[a,b], S. Lo Meo[a,30], S. Marcellini[a], G. Masetti[a], F.L. Navarria[a,b], A. Perrotta[a], F. Primavera[a,b], A.M. Rossi[a,b], T. Rovelli[a,b], G.P. Siroli[a,b], N. Tosi[a]

INFN Sezione di Catania [a], Università di Catania [b], Catania, Italy

S. Albergo[a,b,31], S. Costa[a,b], A. Di Mattia[a], R. Potenza[a,b], A. Tricomi[a,b,31], C. Tuve[a,b]

INFN Sezione di Firenze [a], Università di Firenze [b], Firenze, Italy

G. Barbagli[a], R. Ceccarelli, K. Chatterjee[a,b], V. Ciulli[a,b], C. Civinini[a], R. D'Alessandro[a,b], E. Focardi[a,b], G. Latino, P. Lenzi[a,b], M. Meschini[a], S. Paoletti[a], L. Russo[a,32], G. Sguazzoni[a], D. Strom[a], L. Viliani[a]

INFN Laboratori Nazionali di Frascati, Frascati, Italy

L. Benussi, S. Bianco, D. Piccolo

INFN Sezione di Genova [a], Università di Genova [b], Genova, Italy

M. Bozzo[a,b], F. Ferro[a], R. Mulargia[a,b], E. Robutti[a], S. Tosi[a,b]

INFN Sezione di Milano-Bicocca [a], Università di Milano-Bicocca [b], Milano, Italy

A. Benaglia[a], A. Beschi[a,b], F. Brivio[a,b], V. Ciriolo[a,b,18], S. Di Guida[a,b,18], M.E. Dinardo[a,b], P. Dini[a], S. Fiorendi[a,b], S. Gennai[a], A. Ghezzi[a,b], P. Govoni[a,b], L. Guzzi[a,b], M. Malberti[a], S. Malvezzi[a], D. Menasce[a], F. Monti[a,b], L. Moroni[a], G. Ortona[a,b], M. Paganoni[a,b], D. Pedrini[a], S. Ragazzi[a,b], T. Tabarelli de Fatis[a,b], D. Zuolo[a,b]

INFN Sezione di Napoli [a], Università di Napoli 'Federico II' [b], Napoli, Italy, Università della Basilicata [c], Potenza, Italy, Università G. Marconi [d], Roma, Italy

S. Buontempo[a], N. Cavallo[a,c], A. De Iorio[a,b], A. Di Crescenzo[a,b], F. Fabozzi[a,c], F. Fienga[a], G. Galati[a], A.O.M. Iorio[a,b], L. Lista[a,b], S. Meola[a,d,18], P. Paolucci[a,18], B. Rossi[a], C. Sciacca[a,b], E. Voevodina[a,b]

INFN Sezione di Padova [a], Università di Padova [b], Padova, Italy, Università di Trento [c], Trento, Italy

P. Azzi[a], N. Bacchetta[a], D. Bisello[a,b], A. Boletti[a,b], A. Bragagnolo, R. Carlin[a,b], P. Checchia[a], P. De Castro Manzano[a], T. Dorigo[a], U. Dosselli[a], F. Gasparini[a,b], U. Gasparini[a,b], A. Gozzelino[a], S.Y. Hoh, P. Lujan, M. Margoni[a,b], A.T. Meneguzzo[a,b], J. Pazzini[a,b], M. Presilla[b], P. Ronchese[a,b], R. Rossin[a,b], F. Simonetto[a,b], A. Tiko, M. Tosi[a,b], M. Zanetti[a,b], P. Zotto[a,b], G. Zumerle[a,b]

INFN Sezione di Pavia [a], Università di Pavia [b], Pavia, Italy

A. Braghieri[a], P. Montagna[a,b], S.P. Ratti[a,b], V. Re[a], M. Ressegotti[a,b], C. Riccardi[a,b], P. Salvini[a], I. Vai[a,b], P. Vitulo[a,b]

INFN Sezione di Perugia [a], Università di Perugia [b], Perugia, Italy

M. Biasini[a,b], G.M. Bilei[a], C. Cecchi[a,b], D. Ciangottini[a,b], L. Fanò[a,b], P. Lariccia[a,b], R. Leonardi[a,b], E. Manoni[a], G. Mantovani[a,b], V. Mariani[a,b], M. Menichelli[a], A. Rossi[a,b], A. Santocchia[a,b], D. Spiga[a]

INFN Sezione di Pisa ^{a}, Università di Pisa ^{b}, Scuola Normale Superiore di Pisa ^{c}, Pisa, Italy

K. Androsov^a, P. Azzurri^a, G. Bagliesi^a, V. Bertacchi^{a,c}, L. Bianchini^a, T. Boccali^a, R. Castaldi^a, M.A. Ciocci^{a,b}, R. Dell'Orso^a, G. Fedi^a, F. Fiori^{a,c}, L. Giannini^{a,c}, A. Giassi^a, M.T. Grippo^a, F. Ligabue^{a,c}, E. Manca^{a,c}, G. Mandorli^{a,c}, A. Messineo^{a,b}, F. Palla^a, A. Rizzi^{a,b}, G. Rolandi^{33}, A. Scribano^a, P. Spagnolo^a, R. Tenchini^a, G. Tonelli^{a,b}, N. Turini, A. Venturi^a, P.G. Verdini^a

INFN Sezione di Roma ^{a}, Sapienza Università di Roma ^{b}, Rome, Italy

F. Cavallari^a, M. Cipriani^{a,b}, D. Del Re^{a,b}, E. Di Marco^{a,b}, M. Diemoz^a, E. Longo^{a,b}, B. Marzocchi^{a,b}, P. Meridiani^a, G. Organtini^{a,b}, F. Pandolfi^a, R. Paramatti^{a,b}, C. Quaranta^{a,b}, S. Rahatlou^{a,b}, C. Rovelli^a, F. Santanastasio^{a,b}, L. Soffi^{a,b}

INFN Sezione di Torino ^{a}, Università di Torino ^{b}, Torino, Italy, Università del Piemonte Orientale ^{c}, Novara, Italy

N. Amapane^{a,b}, R. Arcidiacono^{a,c}, S. Argiro^{a,b}, M. Arneodo^{a,c}, N. Bartosik^a, R. Bellan^{a,b}, C. Biino^a, A. Cappati^{a,b}, N. Cartiglia^a, S. Cometti^a, M. Costa^{a,b}, R. Covarelli^{a,b}, N. Demaria^a, B. Kiani^{a,b}, C. Mariotti^a, S. Maselli^a, E. Migliore^{a,b}, V. Monaco^{a,b}, E. Monteil^{a,b}, M. Monteno^a, M.M. Obertino^{a,b}, L. Pacher^{a,b}, N. Pastrone^a, M. Pelliccioni^a, G.L. Pinna Angioni^{a,b}, A. Romero^{a,b}, M. Ruspa^{a,c}, R. Sacchi^{a,b}, R. Salvatico^{a,b}, K. Shchelina^{a,b}, V. Sola^a, A. Solano^{a,b}, D. Soldi^{a,b}, A. Staiano^a

INFN Sezione di Trieste ^{a}, Università di Trieste ^{b}, Trieste, Italy

S. Belforte^a, V. Candelise^{a,b}, M. Casarsa^a, F. Cossutti^a, A. Da Rold^{a,b}, G. Della Ricca^{a,b}, F. Vazzoler^{a,b}, A. Zanetti^a

Kyungpook National University, Daegu, Korea

B. Kim, D.H. Kim, G.N. Kim, M.S. Kim, J. Lee, S.W. Lee, C.S. Moon, Y.D. Oh, S.I. Pak, S. Sekmen, D.C. Son, Y.C. Yang

Chonnam National University, Institute for Universe and Elementary Particles, Kwangju, Korea

H. Kim, D.H. Moon, G. Oh

Hanyang University, Seoul, Korea

B. Francois, T.J. Kim, J. Park

Korea University, Seoul, Korea

S. Cho, S. Choi, Y. Go, D. Gyun, S. Ha, B. Hong, K. Lee, K.S. Lee, J. Lim, J. Park, S.K. Park, Y. Roh

Kyung Hee University, Department of Physics

J. Goh

Sejong University, Seoul, Korea

H.S. Kim

Seoul National University, Seoul, Korea

J. Almond, J.H. Bhyun, J. Choi, S. Jeon, J. Kim, J.S. Kim, H. Lee, K. Lee, S. Lee, K. Nam, S.B. Oh, B.C. Radburn-Smith, S.h. Seo, U.K. Yang, H.D. Yoo, I. Yoon, G.B. Yu

University of Seoul, Seoul, Korea

D. Jeon, H. Kim, J.H. Kim, J.S.H. Lee, I.C. Park, I. Watson

Sungkyunkwan University, Suwon, Korea

Y. Choi, C. Hwang, Y. Jeong, J. Lee, Y. Lee, I. Yu

Riga Technical University, Riga, Latvia

V. Veckalns[34]

Vilnius University, Vilnius, Lithuania

V. Dudenas, A. Juodagalvis, J. Vaitkus

National Centre for Particle Physics, Universiti Malaya, Kuala Lumpur, Malaysia

Z.A. Ibrahim, F. Mohamad Idris[35], W.A.T. Wan Abdullah, M.N. Yusli, Z. Zolkapli

Universidad de Sonora (UNISON), Hermosillo, Mexico

J.F. Benitez, A. Castaneda Hernandez, J.A. Murillo Quijada, L. Valencia Palomo

Centro de Investigacion y de Estudios Avanzados del IPN, Mexico City, Mexico

H. Castilla-Valdez, E. De La Cruz-Burelo, I. Heredia-De La Cruz[36], R. Lopez-Fernandez, A. Sanchez-Hernandez

Universidad Iberoamericana, Mexico City, Mexico

S. Carrillo Moreno, C. Oropeza Barrera, M. Ramirez-Garcia, F. Vazquez Valencia

Benemerita Universidad Autonoma de Puebla, Puebla, Mexico

J. Eysermans, I. Pedraza, H.A. Salazar Ibarguen, C. Uribe Estrada

Universidad Autónoma de San Luis Potosí, San Luis Potosí, Mexico

A. Morelos Pineda

University of Montenegro, Podgorica, Montenegro

N. Raicevic

University of Auckland, Auckland, New Zealand

D. Krofcheck

University of Canterbury, Christchurch, New Zealand

S. Bheesette, P.H. Butler

National Centre for Physics, Quaid-I-Azam University, Islamabad, Pakistan

A. Ahmad, M. Ahmad, Q. Hassan, H.R. Hoorani, W.A. Khan, M.A. Shah, M. Shoaib, M. Waqas

AGH University of Science and Technology Faculty of Computer Science, Electronics and Telecommunications, Krakow, Poland

V. Avati, L. Grzanka, M. Malawski

National Centre for Nuclear Research, Swierk, Poland

H. Bialkowska, M. Bluj, B. Boimska, M. Górski, M. Kazana, M. Szleper, P. Zalewski

Institute of Experimental Physics, Faculty of Physics, University of Warsaw, Warsaw, Poland

K. Bunkowski, A. Byszuk[37], K. Doroba, A. Kalinowski, M. Konecki, J. Krolikowski, M. Misiura, M. Olszewski, A. Pyskir, M. Walczak

Laboratório de Instrumentação e Física Experimental de Partículas, Lisboa, Portugal

M. Araujo, P. Bargassa, D. Bastos, A. Di Francesco, P. Faccioli, B. Galinhas, M. Gallinaro, J. Hollar, N. Leonardo, J. Seixas, G. Strong, O. Toldaiev, J. Varela

Joint Institute for Nuclear Research, Dubna, Russia

S. Afanasiev, P. Bunin, M. Gavrilenko, I. Golutvin, I. Gorbunov, A. Kamenev, V. Karjavine, A. Lanev, A. Malakhov, V. Matveev[38,39], P. Moisenz, V. Palichik, V. Perelygin, M. Savina, S. Shmatov, S. Shulha, N. Skatchkov, V. Smirnov, N. Voytishin, A. Zarubin

Petersburg Nuclear Physics Institute, Gatchina (St. Petersburg), Russia

L. Chtchipounov, V. Golovtsov, Y. Ivanov, V. Kim[40], E. Kuznetsova[41], P. Levchenko, V. Murzin, V. Oreshkin, I. Smirnov, D. Sosnov, V. Sulimov, L. Uvarov, A. Vorobyev

Institute for Nuclear Research, Moscow, Russia

Yu. Andreev, A. Dermenev, S. Gninenko, N. Golubev, A. Karneyeu, M. Kirsanov, N. Krasnikov, A. Pashenkov, D. Tlisov, A. Toropin

Institute for Theoretical and Experimental Physics named by A.I. Alikhanov of NRC 'Kurchatov Institute', Moscow, Russia

V. Epshteyn, V. Gavrilov, N. Lychkovskaya, A. Nikitenko[42], V. Popov, I. Pozdnyakov, G. Safronov, A. Spiridonov, A. Stepennov, M. Toms, E. Vlasov, A. Zhokin

Moscow Institute of Physics and Technology, Moscow, Russia

T. Aushev

National Research Nuclear University 'Moscow Engineering Physics Institute' (MEPhI), Moscow, Russia

M. Chadeeva[43], P. Parygin, E. Popova, V. Rusinov

P.N. Lebedev Physical Institute, Moscow, Russia

V. Andreev, M. Azarkin, I. Dremin[39], M. Kirakosyan, A. Terkulov

Skobeltsyn Institute of Nuclear Physics, Lomonosov Moscow State University, Moscow, Russia

A. Belyaev, E. Boos, V. Bunichev, M. Dubinin[44], L. Dudko, A. Ershov, A. Gribushin, V. Klyukhin, O. Kodolova, I. Lokhtin, S. Obraztsov, M. Perfilov, V. Savrin

Novosibirsk State University (NSU), Novosibirsk, Russia

A. Barnyakov[45], V. Blinov[45], T. Dimova[45], L. Kardapoltsev[45], Y. Skovpen[45]

Institute for High Energy Physics of National Research Centre 'Kurchatov Institute', Protvino, Russia

I. Azhgirey, I. Bayshev, S. Bitioukov, V. Kachanov, D. Konstantinov, P. Mandrik, V. Petrov, R. Ryutin, S. Slabospitskii, A. Sobol, S. Troshin, N. Tyurin, A. Uzunian, A. Volkov

National Research Tomsk Polytechnic University, Tomsk, Russia

A. Babaev, A. Iuzhakov, V. Okhotnikov

Tomsk State University, Tomsk, Russia

V. Borchsh, V. Ivanchenko, E. Tcherniaev

University of Belgrade: Faculty of Physics and VINCA Institute of Nuclear Sciences

P. Adzic[46], P. Cirkovic, D. Devetak, M. Dordevic, P. Milenovic, J. Milosevic, M. Stojanovic

Centro de Investigaciones Energéticas Medioambientales y Tecnológicas (CIEMAT), Madrid, Spain

M. Aguilar-Benitez, J. Alcaraz Maestre, A. Álvarez Fernández, I. Bachiller, M. Barrio Luna, J.A. Brochero Cifuentes, C.A. Carrillo Montoya, M. Cepeda, M. Cerrada, N. Colino, B. De La Cruz, A. Delgado Peris, C. Fernandez Bedoya, J.P. Fernández Ramos, J. Flix, M.C. Fouz, O. Gonzalez Lopez, S. Goy Lopez, J.M. Hernandez, M.I. Josa, D. Moran, Á. Navarro Tobar, A. Pérez-Calero Yzquierdo, J. Puerta Pelayo, I. Redondo, L. Romero, S. Sánchez Navas, M.S. Soares, A. Triossi, C. Willmott

Universidad Autónoma de Madrid, Madrid, Spain

C. Albajar, J.F. de Trocóniz

Universidad de Oviedo, Instituto Universitario de Ciencias y Tecnologías Espaciales de Asturias (ICTEA), Oviedo, Spain

B. Alvarez Gonzalez, J. Cuevas, C. Erice, J. Fernandez Menendez, S. Folgueras, I. Gonzalez Caballero, J.R. González Fernández, E. Palencia Cortezon, V. Rodríguez Bouza, S. Sanchez Cruz

Instituto de Física de Cantabria (IFCA), CSIC-Universidad de Cantabria, Santander, Spain

I.J. Cabrillo, A. Calderon, B. Chazin Quero, J. Duarte Campderros, M. Fernandez, P.J. Fernández Manteca, A. García Alonso, G. Gomez, C. Martinez Rivero, P. Martinez Ruiz del Arbol, F. Matorras, J. Piedra Gomez, C. Prieels, T. Rodrigo, A. Ruiz-Jimeno, L. Scodellaro, N. Trevisani, I. Vila, J.M. Vizan Garcia

University of Colombo, Colombo, Sri Lanka

K. Malagalage

University of Ruhuna, Department of Physics, Matara, Sri Lanka

W.G.D. Dharmaratna, N. Wickramage

CERN, European Organization for Nuclear Research, Geneva, Switzerland

D. Abbaneo, B. Akgun, E. Auffray, G. Auzinger, J. Baechler, P. Baillon, A.H. Ball, D. Barney, J. Bendavid, M. Bianco, A. Bocci, E. Bossini, C. Botta, E. Brondolin, T. Camporesi, A. Caratelli, G. Cerminara, E. Chapon, G. Cucciati, D. d'Enterria, A. Dabrowski, N. Daci, V. Daponte, A. David, A. De Roeck, N. Deelen, M. Deile, M. Dobson, M. Dünser, N. Dupont, A. Elliott-Peisert, F. Fallavollita[47], D. Fasanella, G. Franzoni, J. Fulcher, W. Funk, S. Giani, D. Gigi, A. Gilbert, K. Gill, F. Glege, M. Gruchala, M. Guilbaud, D. Gulhan, J. Hegeman, C. Heidegger, Y. Iiyama, V. Innocente, A. Jafari, P. Janot, O. Karacheban[21], J. Kaspar, J. Kieseler, M. Krammer[1], C. Lange, P. Lecoq, C. Lourenço, L. Malgeri, M. Mannelli, A. Massironi, F. Meijers, J.A. Merlin, S. Mersi, E. Meschi, F. Moortgat, M. Mulders, J. Ngadiuba, S. Nourbakhsh, S. Orfanelli, L. Orsini, F. Pantaleo[18], L. Pape, E. Perez, M. Peruzzi, A. Petrilli, G. Petrucciani, A. Pfeiffer, M. Pierini, F.M. Pitters, M. Quinto, D. Rabady, A. Racz, M. Rovere, H. Sakulin, C. Schäfer, C. Schwick, M. Selvaggi, A. Sharma, P. Silva, W. Snoeys, P. Sphicas[48], J. Steggemann, V.R. Tavolaro, D. Treille, A. Tsirou, A. Vartak, M. Verzetti, W.D. Zeuner

Paul Scherrer Institut, Villigen, Switzerland

L. Caminada[49], K. Deiters, W. Erdmann, R. Horisberger, Q. Ingram, H.C. Kaestli, D. Kotlinski, U. Langenegger, T. Rohe, S.A. Wiederkehr

ETH Zurich — Institute for Particle Physics and Astrophysics (IPA), Zurich, Switzerland

M. Backhaus, P. Berger, N. Chernyavskaya, G. Dissertori, M. Dittmar, M. Donegà, C. Dorfer, T.A. Gómez Espinosa, C. Grab, D. Hits, T. Klijnsma, W. Lustermann, R.A. Manzoni, M. Marionneau, M.T. Meinhard, F. Micheli, P. Musella, F. Nessi-Tedaldi, F. Pauss, G. Perrin, L. Perrozzi, S. Pigazzini, M. Reichmann, C. Reissel, T. Reitenspiess, D. Ruini, D.A. Sanz Becerra, M. Schönenberger, L. Shchutska, M.L. Vesterbacka Olsson, R. Wallny, D.H. Zhu

Universität Zürich, Zurich, Switzerland

T.K. Aarrestad, C. Amsler[50], D. Brzhechko, M.F. Canelli, A. De Cosa, R. Del Burgo, S. Donato, C. Galloni, B. Kilminster, S. Leontsinis, V.M. Mikuni, I. Neutelings, G. Rauco, P. Robmann, D. Salerno, K. Schweiger, C. Seitz, Y. Takahashi, S. Wertz, A. Zucchetta

National Central University, Chung-Li, Taiwan

T.H. Doan, C.M. Kuo, W. Lin, S.S. Yu

National Taiwan University (NTU), Taipei, Taiwan

P. Chang, Y. Chao, K.F. Chen, P.H. Chen, W.-S. Hou, Y.y. Li, R.-S. Lu, E. Paganis, A. Psallidas, A. Steen

Chulalongkorn University, Faculty of Science, Department of Physics, Bangkok, Thailand

B. Asavapibhop, N. Srimanobhas, N. Suwonjandee

Çukurova University, Physics Department, Science and Art Faculty, Adana, Turkey

A. Bat, F. Boran, S. Cerci[51], S. Damarseckin[52], Z.S. Demiroglu, F. Dolek, C. Dozen, I. Dumanoglu, G. Gokbulut, EmineGurpinar Guler[53], Y. Guler, I. Hos[54], C. Isik, E.E. Kangal[55], O. Kara, A. Kayis Topaksu, U. Kiminsu, M. Oglakci, G. Onengut, K. Ozdemir[56], S. Ozturk[57], A.E. Simsek, D. Sunar Cerci[51], U.G. Tok, S. Turkcapar, I.S. Zorbakir, C. Zorbilmez

Middle East Technical University, Physics Department, Ankara, Turkey

B. Isildak[58], G. Karapinar[59], M. Yalvac

Bogazici University, Istanbul, Turkey

I.O. Atakisi, E. Gülmez, M. Kaya[60], O. Kaya[61], B. Kaynak, Ö. Özçelik, S. Ozkorucuklu[62], S. Tekten, E.A. Yetkin[63]

Istanbul Technical University, Istanbul, Turkey

A. Cakir, K. Cankocak, Y. Komurcu, S. Sen[64]

Institute for Scintillation Materials of National Academy of Science of Ukraine, Kharkov, Ukraine

B. Grynyov

National Scientific Center, Kharkov Institute of Physics and Technology, Kharkov, Ukraine

L. Levchuk

University of Bristol, Bristol, United Kingdom

F. Ball, E. Bhal, S. Bologna, J.J. Brooke, D. Burns, E. Clement, D. Cussans, O. Davignon, H. Flacher, J. Goldstein, G.P. Heath, H.F. Heath, L. Kreczko, S. Paramesvaran, B. Penning, T. Sakuma, S. Seif El Nasr-Storey, D. Smith, V.J. Smith, J. Taylor, A. Titterton

Rutherford Appleton Laboratory, Didcot, United Kingdom

K.W. Bell, A. Belyaev[65], C. Brew, R.M. Brown, D. Cieri, D.J.A. Cockerill, J.A. Coughlan, K. Harder, S. Harper, J. Linacre, K. Manolopoulos, D.M. Newbold, E. Olaiya, D. Petyt, T. Reis, T. Schuh, C.H. Shepherd-Themistocleous, A. Thea, I.R. Tomalin, T. Williams, W.J. Womersley

Imperial College, London, United Kingdom

R. Bainbridge, P. Bloch, J. Borg, S. Breeze, O. Buchmuller, A. Bundock, GurpreetSingh CHAHAL[66], D. Colling, P. Dauncey, G. Davies, M. Della Negra, R. Di Maria, P. Everaerts, G. Hall, G. Iles, T. James, M. Komm, C. Laner, L. Lyons, A.-M. Magnan, S. Malik, A. Martelli, V. Milosevic, J. Nash[67], V. Palladino, M. Pesaresi, D.M. Raymond, A. Richards, A. Rose, E. Scott, C. Seez, A. Shtipliyski, M. Stoye, T. Strebler, S. Summers, A. Tapper, K. Uchida, T. Virdee[18], N. Wardle, D. Winterbottom, J. Wright, A.G. Zecchinelli, S.C. Zenz

Brunel University, Uxbridge, United Kingdom

J.E. Cole, P.R. Hobson, A. Khan, P. Kyberd, C.K. Mackay, A. Morton, I.D. Reid, L. Teodorescu, S. Zahid

Baylor University, Waco, U.S.A.

K. Call, J. Dittmann, K. Hatakeyama, C. Madrid, B. McMaster, N. Pastika, C. Smith

Catholic University of America, Washington, DC, U.S.A.

R. Bartek, A. Dominguez, R. Uniyal

The University of Alabama, Tuscaloosa, U.S.A.

A. Buccilli, S.I. Cooper, C. Henderson, P. Rumerio, C. West

Boston University, Boston, U.S.A.

D. Arcaro, T. Bose, Z. Demiragli, D. Gastler, S. Girgis, D. Pinna, C. Richardson, J. Rohlf, D. Sperka, I. Suarez, L. Sulak, D. Zou

Brown University, Providence, U.S.A.

G. Benelli, B. Burkle, X. Coubez, D. Cutts, M. Hadley, J. Hakala, U. Heintz, J.M. Hogan[68], K.H.M. Kwok, E. Laird, G. Landsberg, J. Lee, Z. Mao, M. Narain, S. Sagir[69], R. Syarif, E. Usai, D. Yu

University of California, Davis, Davis, U.S.A.

R. Band, C. Brainerd, R. Breedon, M. Calderon De La Barca Sanchez, M. Chertok, J. Conway, R. Conway, P.T. Cox, R. Erbacher, C. Flores, G. Funk, F. Jensen, W. Ko, O. Kukral, R. Lander, M. Mulhearn, D. Pellett, J. Pilot, M. Shi, D. Stolp, D. Taylor, K. Tos, M. Tripathi, Z. Wang, F. Zhang

University of California, Los Angeles, U.S.A.

M. Bachtis, C. Bravo, R. Cousins, A. Dasgupta, A. Florent, J. Hauser, M. Ignatenko, N. Mccoll, S. Regnard, D. Saltzberg, C. Schnaible, B. Stone, V. Valuev

University of California, Riverside, Riverside, U.S.A.

K. Burt, R. Clare, J.W. Gary, S.M.A. Ghiasi Shirazi, G. Hanson, G. Karapostoli, E. Kennedy, O.R. Long, M. Olmedo Negrete, M.I. Paneva, W. Si, L. Wang, H. Wei, S. Wimpenny, B.R. Yates, Y. Zhang

University of California, San Diego, La Jolla, U.S.A.

J.G. Branson, P. Chang, S. Cittolin, M. Derdzinski, R. Gerosa, D. Gilbert, B. Hashemi, D. Klein, V. Krutelyov, J. Letts, M. Masciovecchio, S. May, S. Padhi, M. Pieri, V. Sharma, M. Tadel, F. Würthwein, A. Yagil, G. Zevi Della Porta

University of California, Santa Barbara — Department of Physics, Santa Barbara, U.S.A.

N. Amin, R. Bhandari, C. Campagnari, M. Citron, V. Dutta, M. Franco Sevilla, L. Gouskos, J. Incandela, B. Marsh, H. Mei, A. Ovcharova, H. Qu, J. Richman, U. Sarica, D. Stuart, S. Wang, J. Yoo

California Institute of Technology, Pasadena, U.S.A.

D. Anderson, A. Bornheim, J.M. Lawhorn, N. Lu, H.B. Newman, T.Q. Nguyen, J. Pata, M. Spiropulu, J.R. Vlimant, S. Xie, Z. Zhang, R.Y. Zhu

Carnegie Mellon University, Pittsburgh, U.S.A.

M.B. Andrews, T. Ferguson, T. Mudholkar, M. Paulini, M. Sun, I. Vorobiev, M. Weinberg

University of Colorado Boulder, Boulder, U.S.A.

J.P. Cumalat, W.T. Ford, A. Johnson, E. MacDonald, T. Mulholland, R. Patel, A. Perloff, K. Stenson, K.A. Ulmer, S.R. Wagner

Cornell University, Ithaca, U.S.A.

J. Alexander, J. Chaves, Y. Cheng, J. Chu, A. Datta, A. Frankenthal, K. Mcdermott, N. Mirman, J.R. Patterson, D. Quach, A. Rinkevicius[70], A. Ryd, S.M. Tan, Z. Tao, J. Thom, P. Wittich, M. Zientek

Fermi National Accelerator Laboratory, Batavia, U.S.A.

S. Abdullin, M. Albrow, M. Alyari, G. Apollinari, A. Apresyan, A. Apyan, S. Banerjee, L.A.T. Bauerdick, A. Beretvas, J. Berryhill, P.C. Bhat, K. Burkett, J.N. Butler, A. Canepa, G.B. Cerati, H.W.K. Cheung, F. Chlebana, M. Cremonesi, J. Duarte, V.D. Elvira, J. Freeman, Z. Gecse, E. Gottschalk, L. Gray, D. Green, S. Grünendahl, O. Gutsche, AllisonReinsvold Hall, J. Hanlon, R.M. Harris, S. Hasegawa, R. Heller, J. Hirschauer, B. Jayatilaka, S. Jindariani, M. Johnson, U. Joshi, B. Klima, M.J. Kortelainen, B. Kreis, S. Lammel, J. Lewis, D. Lincoln, R. Lipton, M. Liu, T. Liu, J. Lykken, K. Maeshima, J.M. Marraffino, D. Mason, P. McBride, P. Merkel, S. Mrenna, S. Nahn, V. O'Dell, V. Papadimitriou, K. Pedro, C. Pena, G. Rakness, F. Ravera, L. Ristori, B. Schneider, E. Sexton-Kennedy, N. Smith, A. Soha, W.J. Spalding, L. Spiegel, S. Stoynev, J. Strait, N. Strobbe, L. Taylor, S. Tkaczyk, N.V. Tran, L. Uplegger, E.W. Vaandering, C. Vernieri, M. Verzocchi, R. Vidal, M. Wang, H.A. Weber

University of Florida, Gainesville, U.S.A.

D. Acosta, P. Avery, P. Bortignon, D. Bourilkov, A. Brinkerhoff, L. Cadamuro, A. Carnes, V. Cherepanov, D. Curry, F. Errico, R.D. Field, S.V. Gleyzer, B.M. Joshi, M. Kim, J. Konigsberg, A. Korytov, K.H. Lo, P. Ma, K. Matchev, N. Menendez, G. Mitselmakher, D. Rosenzweig, K. Shi, J. Wang, S. Wang, X. Zuo

Florida International University, Miami, U.S.A.

Y.R. Joshi

Florida State University, Tallahassee, U.S.A.

T. Adams, A. Askew, S. Hagopian, V. Hagopian, K.F. Johnson, R. Khurana, T. Kolberg, G. Martinez, T. Perry, H. Prosper, C. Schiber, R. Yohay, J. Zhang

Florida Institute of Technology, Melbourne, U.S.A.

M.M. Baarmand, V. Bhopatkar, M. Hohlmann, D. Noonan, M. Rahmani, M. Saunders, F. Yumiceva

University of Illinois at Chicago (UIC), Chicago, U.S.A.

M.R. Adams, L. Apanasevich, D. Berry, R.R. Betts, R. Cavanaugh, X. Chen, S. Dittmer, O. Evdokimov, C.E. Gerber, D.A. Hangal, D.J. Hofman, K. Jung, C. Mills, T. Roy, M.B. Tonjes, N. Varelas, H. Wang, X. Wang, Z. Wu

The University of Iowa, Iowa City, U.S.A.

M. Alhusseini, B. Bilki[53], W. Clarida, K. Dilsiz[71], S. Durgut, R.P. Gandrajula, M. Haytmyradov, V. Khristenko, O.K. Köseyan, J.-P. Merlo, A. Mestvirishvili[72], A. Moeller, J. Nachtman, H. Ogul[73], Y. Onel, F. Ozok[74], A. Penzo, C. Snyder, E. Tiras, J. Wetzel

Johns Hopkins University, Baltimore, U.S.A.

B. Blumenfeld, A. Cocoros, N. Eminizer, D. Fehling, L. Feng, A.V. Gritsan, W.T. Hung, P. Maksimovic, J. Roskes, M. Swartz, M. Xiao

The University of Kansas, Lawrence, U.S.A.

C. Baldenegro Barrera, P. Baringer, A. Bean, S. Boren, J. Bowen, A. Bylinkin, T. Isidori, S. Khalil, J. King, A. Kropivnitskaya, C. Lindsey, D. Majumder, W. Mcbrayer, N. Minafra, M. Murray, C. Rogan, C. Royon, S. Sanders, E. Schmitz, J.D. Tapia Takaki, Q. Wang, J. Williams

Kansas State University, Manhattan, U.S.A.

S. Duric, A. Ivanov, K. Kaadze, D. Kim, Y. Maravin, D.R. Mendis, T. Mitchell, A. Modak, A. Mohammadi

Lawrence Livermore National Laboratory, Livermore, U.S.A.

F. Rebassoo, D. Wright

University of Maryland, College Park, U.S.A.

A. Baden, O. Baron, A. Belloni, S.C. Eno, Y. Feng, N.J. Hadley, S. Jabeen, G.Y. Jeng, R.G. Kellogg, J. Kunkle, A.C. Mignerey, S. Nabili, F. Ricci-Tam, M. Seidel, Y.H. Shin, A. Skuja, S.C. Tonwar, K. Wong

Massachusetts Institute of Technology, Cambridge, U.S.A.

D. Abercrombie, B. Allen, A. Baty, R. Bi, S. Brandt, W. Busza, I.A. Cali, M. D'Alfonso, G. Gomez Ceballos, M. Goncharov, P. Harris, D. Hsu, M. Hu, M. Klute, D. Kovalskyi, Y.-J. Lee, P.D. Luckey, B. Maier, A.C. Marini, C. Mcginn, C. Mironov, S. Narayanan, X. Niu, C. Paus, D. Rankin, C. Roland, G. Roland, Z. Shi, G.S.F. Stephans, K. Sumorok, K. Tatar, D. Velicanu, J. Wang, T.W. Wang, B. Wyslouch

University of Minnesota, Minneapolis, U.S.A.

A.C. Benvenuti[†], R.M. Chatterjee, A. Evans, S. Guts, P. Hansen, J. Hiltbrand, S. Kalafut, Y. Kubota, Z. Lesko, J. Mans, R. Rusack, M.A. Wadud

University of Mississippi, Oxford, U.S.A.

J.G. Acosta, S. Oliveros

University of Nebraska-Lincoln, Lincoln, U.S.A.

K. Bloom, D.R. Claes, C. Fangmeier, L. Finco, F. Golf, R. Gonzalez Suarez, R. Kamalieddin, I. Kravchenko, J.E. Siado, G.R. Snow, B. Stieger

State University of New York at Buffalo, Buffalo, U.S.A.

C. Harrington, I. Iashvili, A. Kharchilava, C. Mclean, D. Nguyen, A. Parker, S. Rappoccio, B. Roozbahani

Northeastern University, Boston, U.S.A.

G. Alverson, E. Barberis, C. Freer, Y. Haddad, A. Hortiangtham, G. Madigan, D.M. Morse, T. Orimoto, L. Skinnari, A. Tishelman-Charny, T. Wamorkar, B. Wang, A. Wisecarver, D. Wood

Northwestern University, Evanston, U.S.A.

S. Bhattacharya, J. Bueghly, T. Gunter, K.A. Hahn, N. Odell, M.H. Schmitt, K. Sung, M. Trovato, M. Velasco

University of Notre Dame, Notre Dame, U.S.A.

R. Bucci, N. Dev, R. Goldouzian, M. Hildreth, K. Hurtado Anampa, C. Jessop, D.J. Karmgard, K. Lannon, W. Li, N. Loukas, N. Marinelli, I. Mcalister, F. Meng, C. Mueller, Y. Musienko[38], M. Planer, R. Ruchti, P. Siddireddy, G. Smith, S. Taroni, M. Wayne, A. Wightman, M. Wolf, A. Woodard

The Ohio State University, Columbus, U.S.A.

J. Alimena, B. Bylsma, L.S. Durkin, S. Flowers, B. Francis, C. Hill, W. Ji, A. Lefeld, T.Y. Ling, B.L. Winer

Princeton University, Princeton, U.S.A.

S. Cooperstein, G. Dezoort, P. Elmer, J. Hardenbrook, N. Haubrich, S. Higginbotham, A. Kalogeropoulos, S. Kwan, D. Lange, M.T. Lucchini, J. Luo, D. Marlow, K. Mei, I. Ojalvo, J. Olsen, C. Palmer, P. Piroué, J. Salfeld-Nebgen, D. Stickland, C. Tully, Z. Wang

University of Puerto Rico, Mayaguez, U.S.A.

S. Malik, S. Norberg

Purdue University, West Lafayette, U.S.A.

A. Barker, V.E. Barnes, S. Das, L. Gutay, M. Jones, A.W. Jung, A. Khatiwada, B. Mahakud, D.H. Miller, G. Negro, N. Neumeister, C.C. Peng, S. Piperov, H. Qiu, J.F. Schulte, J. Sun, F. Wang, R. Xiao, W. Xie

Purdue University Northwest, Hammond, U.S.A.

T. Cheng, J. Dolen, N. Parashar

Rice University, Houston, U.S.A.

K.M. Ecklund, S. Freed, F.J.M. Geurts, M. Kilpatrick, Arun Kumar, W. Li, B.P. Padley, R. Redjimi, J. Roberts, J. Rorie, W. Shi, A.G. Stahl Leiton, Z. Tu, A. Zhang

University of Rochester, Rochester, U.S.A.

A. Bodek, P. de Barbaro, R. Demina, Y.t. Duh, J.L. Dulemba, C. Fallon, M. Galanti, A. Garcia-Bellido, J. Han, O. Hindrichs, A. Khukhunaishvili, E. Ranken, P. Tan, R. Taus

Rutgers, The State University of New Jersey, Piscataway, U.S.A.

B. Chiarito, J.P. Chou, A. Gandrakota, Y. Gershtein, E. Halkiadakis, A. Hart, M. Heindl, E. Hughes, S. Kaplan, S. Kyriacou, I. Laflotte, A. Lath, R. Montalvo, K. Nash, M. Osherson, H. Saka, S. Salur, S. Schnetzer, D. Sheffield, S. Somalwar, R. Stone, S. Thomas, P. Thomassen

University of Tennessee, Knoxville, U.S.A.

H. Acharya, A.G. Delannoy, J. Heideman, G. Riley, S. Spanier

Texas A&M University, College Station, U.S.A.

O. Bouhali[75], A. Celik, M. Dalchenko, M. De Mattia, A. Delgado, S. Dildick, R. Eusebi, J. Gilmore, T. Huang, T. Kamon[76], S. Luo, D. Marley, R. Mueller, D. Overton, L. Perniè, D. Rathjens, A. Safonov

Texas Tech University, Lubbock, U.S.A.

N. Akchurin, J. Damgov, F. De Guio, S. Kunori, K. Lamichhane, S.W. Lee, T. Mengke, S. Muthumuni, T. Peltola, S. Undleeb, I. Volobouev, Z. Wang, A. Whitbeck

Vanderbilt University, Nashville, U.S.A.

S. Greene, A. Gurrola, R. Janjam, W. Johns, C. Maguire, A. Melo, H. Ni, K. Padeken, F. Romeo, P. Sheldon, S. Tuo, J. Velkovska, M. Verweij

University of Virginia, Charlottesville, U.S.A.

M.W. Arenton, P. Barria, B. Cox, G. Cummings, R. Hirosky, M. Joyce, A. Ledovskoy, C. Neu, B. Tannenwald, Y. Wang, E. Wolfe, F. Xia

Wayne State University, Detroit, U.S.A.

R. Harr, P.E. Karchin, N. Poudyal, J. Sturdy, P. Thapa, S. Zaleski

University of Wisconsin — Madison, Madison, WI, U.S.A.

J. Buchanan, C. Caillol, D. Carlsmith, S. Dasu, I. De Bruyn, L. Dodd, B. Gomber[77], M. Herndon, A. Hervé, U. Hussain, P. Klabbers, A. Lanaro, A. Loeliger, K. Long, R. Loveless, J. Madhusudanan Sreekala, T. Ruggles, A. Savin, V. Sharma, W.H. Smith, D. Teague, S. Trembath-reichert, N. Woods

†: Deceased
1: Also at Vienna University of Technology, Vienna, Austria
2: Also at IRFU, CEA, Université Paris-Saclay, Gif-sur-Yvette, France
3: Also at Universidade Estadual de Campinas, Campinas, Brazil
4: Also at Federal University of Rio Grande do Sul, Porto Alegre, Brazil
5: Also at UFMS, Nova Andradina, Brazil
6: Also at Universidade Federal de Pelotas, Pelotas, Brazil
7: Also at Université Libre de Bruxelles, Bruxelles, Belgium
8: Also at University of Chinese Academy of Sciences, Beijing, China
9: Also at Institute for Theoretical and Experimental Physics named by A.I. Alikhanov of NRC 'Kurchatov Institute', Moscow, Russia
10: Also at Joint Institute for Nuclear Research, Dubna, Russia
11: Now at Cairo University, Cairo, Egypt

12: Also at British University in Egypt, Cairo, Egypt

13: Now at Ain Shams University, Cairo, Egypt

14: Also at Purdue University, West Lafayette, U.S.A.

15: Also at Université de Haute Alsace, Mulhouse, France

16: Also at Tbilisi State University, Tbilisi, Georgia

17: Also at Erzincan Binali Yildirim University, Erzincan, Turkey

18: Also at CERN, European Organization for Nuclear Research, Geneva, Switzerland

19: Also at RWTH Aachen University, III. Physikalisches Institut A, Aachen, Germany

20: Also at University of Hamburg, Hamburg, Germany

21: Also at Brandenburg University of Technology, Cottbus, Germany

22: Also at Institute of Physics, University of Debrecen, Debrecen, Hungary, Debrecen, Hungary

23: Also at Institute of Nuclear Research ATOMKI, Debrecen, Hungary

24: Also at MTA-ELTE Lendület CMS Particle and Nuclear Physics Group, Eötvös Loránd University, Budapest, Hungary, Budapest, Hungary

25: Also at IIT Bhubaneswar, Bhubaneswar, India, Bhubaneswar, India

26: Also at Institute of Physics, Bhubaneswar, India

27: Also at Shoolini University, Solan, India

28: Also at University of Visva-Bharati, Santiniketan, India

29: Also at Isfahan University of Technology, Isfahan, Iran

30: Also at Italian National Agency for New Technologies, Energy and Sustainable Economic Development, Bologna, Italy

31: Also at Centro Siciliano di Fisica Nucleare e di Struttura Della Materia, Catania, Italy

32: Also at Università degli Studi di Siena, Siena, Italy

33: Also at Scuola Normale e Sezione dell'INFN, Pisa, Italy

34: Also at Riga Technical University, Riga, Latvia, Riga, Latvia

35: Also at Malaysian Nuclear Agency, MOSTI, Kajang, Malaysia

36: Also at Consejo Nacional de Ciencia y Tecnología, Mexico City, Mexico

37: Also at Warsaw University of Technology, Institute of Electronic Systems, Warsaw, Poland

38: Also at Institute for Nuclear Research, Moscow, Russia

39: Now at National Research Nuclear University 'Moscow Engineering Physics Institute' (MEPhI), Moscow, Russia

40: Also at St. Petersburg State Polytechnical University, St. Petersburg, Russia

41: Also at University of Florida, Gainesville, U.S.A.

42: Also at Imperial College, London, United Kingdom

43: Also at P.N. Lebedev Physical Institute, Moscow, Russia

44: Also at California Institute of Technology, Pasadena, U.S.A.

45: Also at Budker Institute of Nuclear Physics, Novosibirsk, Russia

46: Also at Faculty of Physics, University of Belgrade, Belgrade, Serbia

47: Also at INFN Sezione di Pavia [a], Università di Pavia [b], Pavia, Italy, Pavia, Italy

48: Also at National and Kapodistrian University of Athens, Athens, Greece

49: Also at Universität Zürich, Zurich, Switzerland

50: Also at Stefan Meyer Institute for Subatomic Physics, Vienna, Austria, Vienna, Austria

51: Also at Adiyaman University, Adiyaman, Turkey

52: Also at Şırnak University, Sirnak, Turkey

53: Also at Beykent University, Istanbul, Turkey, Istanbul, Turkey

54: Also at Istanbul Aydin University, Istanbul, Turkey

55: Also at Mersin University, Mersin, Turkey

56: Also at Piri Reis University, Istanbul, Turkey